JOURNAL OF PETROLOGY | VOLUME 40 | NUMBER 4 | PAGES 601–627 | 1999

Metamorphic Evolution of Cordierite-Bearing Migmatites from the Bayerische Wald (Variscan Belt, Germany)

ANGELIKA KALT[1]*, ALFONS BERGER[1] AND PETER BLÜMEL[2]

[1]MINERALOGISCHES INSTITUT, UNIVERSITY OF HEIDELBERG, IM NEUENHEIMER FELD 236, D-69120 HEIDELBERG, GERMANY

[2]INSTITUT FÜR MINERALOGIE, PETROGRAPHIE, STRUKTURGEOLOGIE, SCHNITTSPAHNSTRASSE 9, D-64287 DARMSTADT, GERMANY

RECEIVED MARCH 1, 1998; REVISED TYPESCRIPT ACCEPTED SEPTEMBER 25, 1998

A detailed petrological study was carried out on cordierite-bearing migmatites of the Bayerische Wald (Germany, Bohemian Massif, Variscan Belt) to constrain the physical–chemical conditions of metamorphism and partial melting. Four types of migmatites (MIG1–MIG4) can be classified mainly on the basis of field appearance, microstructures and degree of melt extraction. The four migmatite types and their intercalations preserve a range of mineral assemblages and reaction textures that vary with bulk composition. All rocks followed the same clockwise P–T *path, which can be divided into four stages on the basis of reaction textures and garnet zoning patterns. Prograde evolution is characterized by biotite dehydration melting in the absence of an aqueous fluid phase. The operating dehydration melting reactions changed with bulk composition on small scales and produced locally varying modal cordierite, garnet, spinel and orthopyroxene along with melt. Minimum estimates of peak temperatures (800–850°C) and pressure constraints (0·5–0·7 GPa) emerge from experimental results. Phase compositions, however, were last equilibrated on the retrograde part of the* P–T *path but still record very high temperatures close to peak conditions (770–846°C and 0·44–0·51 GPa) as indicated by the results of geothermobarometry (e.g. Na-in-cordierite, garnet–cordierite, garnet–orthopyroxene equilibria). The calculated temperatures are significantly higher than those previously obtained for similar rocks of the Bayerische Wald. The* P–T *path and conditions derived here suggest that high-temperature metamorphism in the Moldanubian zone of the Bohemian Massif was induced by anomalously high heat influx to shallow crustal levels of 15–20 km depth subsequent to Variscan collision and crustal thickening.*

KEY WORDS: *migmatites; cordierite; melting reactions; Bayerischer Wald, Germany*

INTRODUCTION

High-temperature metamorphism accompanied by partial melting and plutonism is a common feature in collisional belts (Bohlen, 1987; Harley, 1989; and references therein). The geodynamic processes responsible for such high temperatures in medium to shallow crustal levels are not yet well understood. They are generally assessed by models that combine the results of experimental petrology with *P–T–t* paths deduced from rocks in collision zones (Thompson & Connolly, 1995, and references therein). This in turn requires precise data on temperatures, pressures and melt production, information that is commonly gained from metamorphic mineral equilibria.

For determining metamorphic temperatures and pressures pelitic and semipelitic rocks are particularly useful. They undergo a number of mineral reactions during prograde and peak metamorphism, thus monitoring the *P–T* path of a crustal segment during an orogenic event (e.g. Brown, 1993), provided a later retrograde overprint has not obliterated earlier features. Moreover, at high temperatures, mineral reactions in pelitic and semipelitic rocks usually involve the breakdown of hydrous phases, allowing for constraints to be placed on the production

*Corresponding author. Fax: ++49 6221 544805.
e-mail: akalt@classic.min.uni-heidelberg.de

of fluids and/or melts. As the presence and abundance of fluids and melts strongly controls the mechanical behaviour of the crust during metamorphism, these constraints are a prerequisite for modelling the tectonothermal evolution of crustal segments during orogenic events.

High-temperature–low-pressure (HT–LP) pelitic to semipelitic gneisses and migmatites are the dominant metamorphic lithologies within the high-grade metamorphic parts of the Variscan Belt in Europe (Fig. 1a). In particular, the Bohemian Massif (Fig. 1b) displays continuous areas with migmatites that have largely escaped the late and post-orogenic hydrothermal alteration commonly observed in many Variscan massifs. For the Bayerische Wald at the southwestern margin of the Bohemian Massif (Figs 1b and 2), first reconnaissance studies of metamorphism were carried out by Schreyer *et al.* (1964), Schreyer & Blümel (1974) and Blümel & Schreyer (1976, 1977), resulting in a subdivision of the area into petrographic (metamorphic) zones and a first estimate of the peak metamorphic conditions (650–730°C, 0·2–0·4 GPa) on the basis of subsolidus phase equilibria.

This paper presents a detailed analysis of metamorphism in pelitic and semipelitic migmatites from the Bayerische Wald. Field relations, reaction textures, mineral chemistry and geothermobarometric data are used to constrain the P–T evolution of the migmatites. Structures and fabrics of the migmatites (including crystallographic and shape orientation data on cordierite, biotite and garnet) and their relation to melting and melt segregation will be presented elsewhere (Berger & Kalt, 1999).

GEOLOGICAL SETTING AND SAMPLE SELECTION

The Bayerische Wald forms part of the Variscan orogenic belt, which resulted from the collision of Laurasia and Gondwana, and several microplates between these, during Devonian to Carboniferous times (Matte, 1986). The Variscan Belt is now deeply eroded and covered by Mesozoic and younger sediments, so that only isolated basement units crop out in central and western Europe (Fig. 1a). The current study is concerned with an area in the Moldanubian zone (Fig. 1a; Kossmat, 1927), characterized by widespread high-temperature metamorphism at low pressures, accompanied by partial melting and extensive plutonism.

In the Bohemian Massif, the Moldanubian zone can be divided into several tectonometamorphic units (Fig. 1b; Matte, 1986; Franke, 1989). Basically, a basement metamorphosed both during the Cadomian and the Variscan tectonothermal events (Teplá–Barrandian unit) can be distinguished from a composite basement that experienced only Variscan metamorphism (the Moldanubian *sensu strictu*, in the following referred to as 'Moldanubian'; Fig. 1b). The latter consists of tectonic klippen bearing high-temperature–high-pressure (HT–HP) granulites, peridotites and eclogites (Gföhl unit; O'Brien & Carswell, 1993; Medaris *et al.*, 1998), of a pelitic to psammitic HT–LP gneiss and migmatite unit (Monotonous series) and of a more variegated gneiss complex with calc-silicates, marbles, and amphibolites (Varied series; Zoubek, 1965). The Monotonous series contains isolated lenses of eclogite that document a collision event in the Moldanubian before HT–LP metamorphism (e.g. Medaris *et al.*, 1995).

The Bayerische Wald (Fig. 2) is located at the southwestern margin of the Bohemian Massif. It consists mainly of metamorphic rocks belonging to the Monotonous series (migmatites and gneisses of pelitic to psammitic composition) that are intruded by granitoids (Fig. 2). In its central part, the Bayerische Wald is crosscut by a late, narrow, NW–SE trending shear zone, referred to as the Pfahl (Fig. 2). Within the Pfahl zone, a mylonitic fabric has been imposed on metamorphic rocks and granites at lower amphibolite to greenschist-facies conditions (Beer, 1981; Masch & Cetin, 1991) on the retrograde path of regional HT–LP metamorphism.

Schreyer & Blümel (1974) and Blümel & Schreyer (1976, 1977) recognized a sequence of six NW–SE trending petrographic zones located between the Teplá–Barrandian in the north and the Pfahl in the south [see fig. 1 of Schreyer & Blümel (1974)]. They suggested increasing metamorphic grade from greenschist-facies conditions within micaschists in the north (biotite–chlorite zone) to conditions of 650–730°C, 0·2–0·4 GPa in migmatites in the south (cordierite–K-feldspar zone and garnet–cordierite–K-feldspar zone). However, field relations between micaschists and migmatites are not exposed and new petrostructural studies in the adjacent Czech part of the Bohemian Massif (Baburek, 1995; Pitra, 1996) suggest the tectonic juxtaposition of several metamorphic units with distinct P–T paths, including an HT–LP unit (migmatites) and an LT–MP unit (micaschists).

Peak metamorphism of the migmatites was dated at 318–322 Ma BP by concordant U–Pb ages of monazite grainsize fractions (Grauert *et al.*, 1974). U–Pb single monazite dating reveals slightly older ages (323–326 Ma; Kalt *et al.*, unpublished data). Cooling of the migmatites below about 300°C is recorded by K–Ar biotite ages of 325–315 Ma (grainsize fractions, Carl *et al.*, 1985; Kreuzer *et al.* 1989) and Ar–Ar biotite ages of 312–315 Ma (single grains; Kalt *et al.*, unpublished data). Intrusion of granitoids in the Bayerische Wald has not been dated yet.

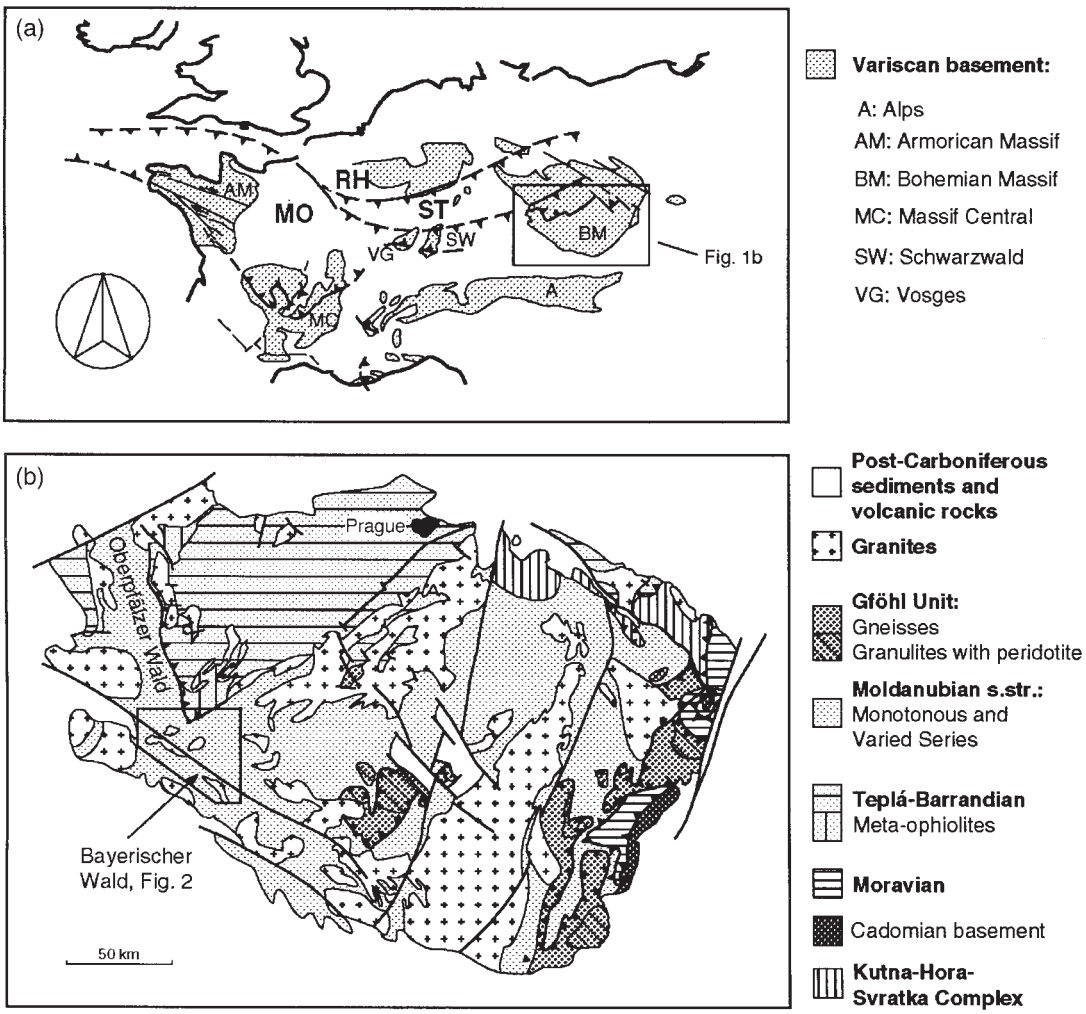

Fig. 1. (a) Outlines of Variscan basement outcrops in Europe, modified after Franke (1989). MO, Moldanubian zone; ST, Saxothuringian zone; RH, Rhenohercynian zone. (b) Simplified geological sketch map of the Moldanubian part of the Bohemian Massif, modified after Medaris *et al.* (1995). Also shown is the area displayed in Fig. 2.

The samples investigated here were all taken from within the cordierite–K-feldspar and the garnet–cordierite–K-feldspar zone of Schreyer & Blümel (1974) and Blümel & Schreyer (1976, 1977). Very fresh and unaltered samples of migmatites were chosen as required for the Na-in-cordierite thermometry (Mirwald, 1986; Kalt *et al.*, 1998) presented here and for the determination of H_2O and CO_2 contents of cordierites presented elsewhere (Kalt, unpublished data). Rocks with the beginning of formation of pinite from cordierite or chlorite from biotite were discarded after inspection with a petrographic microscope. In addition to the cordierite-bearing migmatites, a few associated HT–LP rocks with different compositions were sampled (see section on field relationships). A total of 23 samples were closely investigated in this study.

FIELD RELATIONSHIPS

North and south of the Pfahl, migmatites and various types of gneisses are closely associated (Fig. 2). Gneisses mainly form kilometre-sized bands along strike within the migmatites. The latter may also contain smaller (metre–decimetre scale) lenses or bands of gneisses and amphibolitized calc-silicate rocks and mafic granulites. Whereas migmatites are of pelitic to semipelitic composition and always bear cordierite, gneisses are mainly cordierite free and of psammitic composition. Field features (e.g. boudins, common foliation plane) indicate a common metamorphic history for all lithologies. Granites show irregular and discordant contacts with migmatites and gneisses.

Foliation in the metamorphic rocks is independent of lithology. It strikes mainly NW–SE and dips steeply

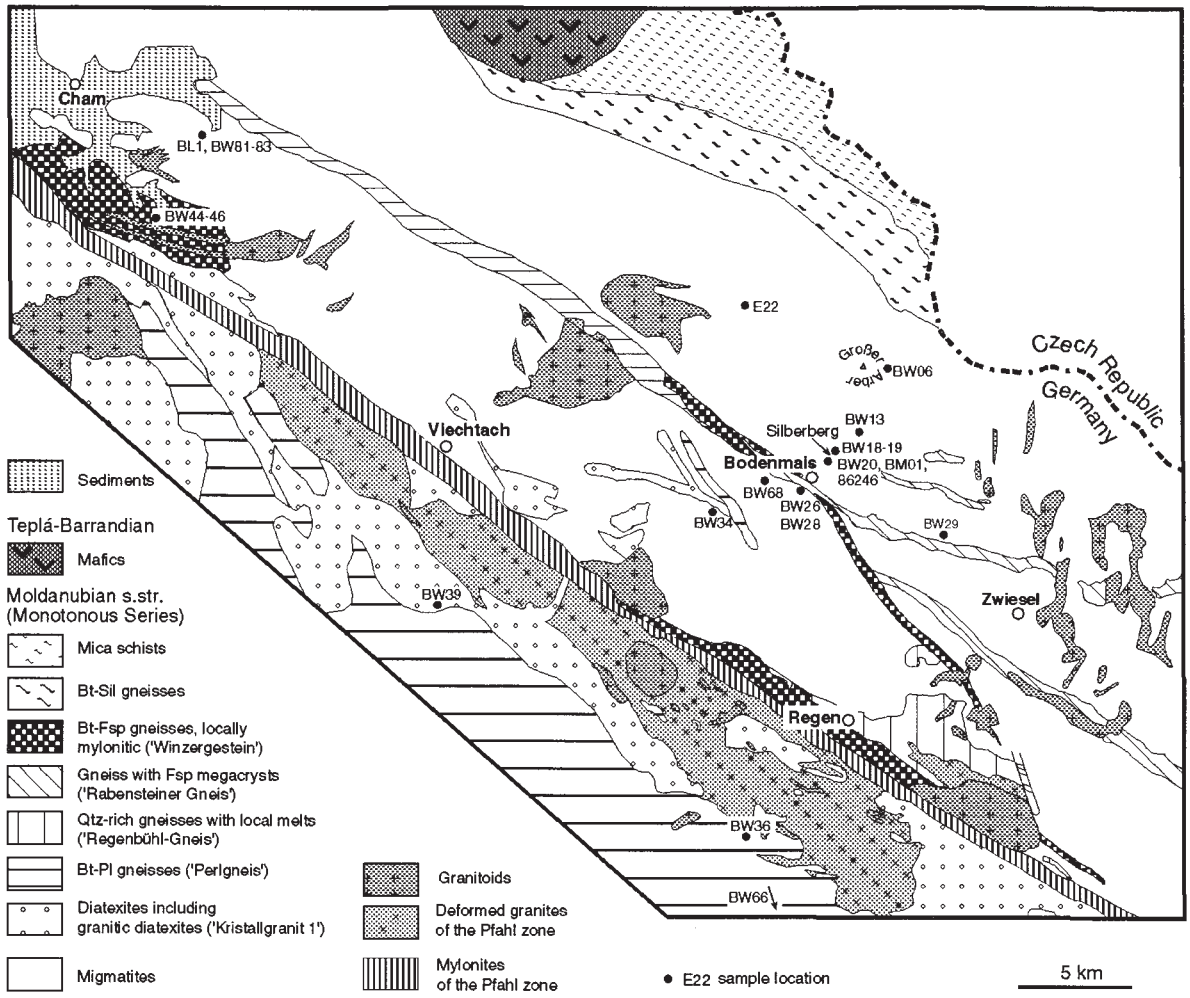

Fig. 2. (a) Simplified geological map of the Bayerische Wald (compare Fig. 1), modified after Troll (1967, 1968) and the Geological Map of Bavaria (1:500 000). (For further explanation, see section on geological setting and sample selection.)

towards the northeast. Other orientations have been locally reported (Fischer & Troll, 1973; Beer, 1981). Stretching lineation, where present, is flat-lying and plunges gently towards ENE or WSW. Small-scale folds (decimetre to metre sized) have rarely been observed and all small-scale folds are bounded by unfolded migmatites. This indicates folding to be a local effect caused by lithological inhomogeneities rather than a regional phenomenon. In addition, foliation trajectories (Fischer & Troll, 1973; Beer, 1981) exclude large-scale folding in the Bayerische Wald, whereas in the adjacent Oberpfälzer Wald (Fig. 1b), foliation trajectories and structures indicate large-scale folding of the migmatites (Tanner & Behrmann, 1995; Behrmann & Tanner, 1997).

Four types of migmatites were distinguished in the Bayerische Wald on the basis of abundance, geometric relationship, modal composition and microstructures of mesosome, melanosome and leucosome (Berger & Kalt, 1999; Fig. 3 and section on petrography). It must be emphasized, however, that these types are 'endmembers' and that also intermediate migmatites may be found. Moreover, all four types are coarse grained (average grainsize 1 mm) and heterogeneous on the millimetre to centimetre scale in terms of mineralogical composition. This is reflected by large ranges in modal compositions within each migmatite type (see section on petrography).

MIG1 types consist only of mesocratic, undifferentiated migmatite. Millimetre- to centimetre-sized and patchy light areas can only be vaguely distinguished from darker areas (Fig. 3a). All other migmatite types are generally stromatic and display foliation subparallel to layering. The widths of mesosomes and leucosomes range from millimetres to several decimetres. Leucosome accounts for 10–40 vol. % of the exposed rock depending on

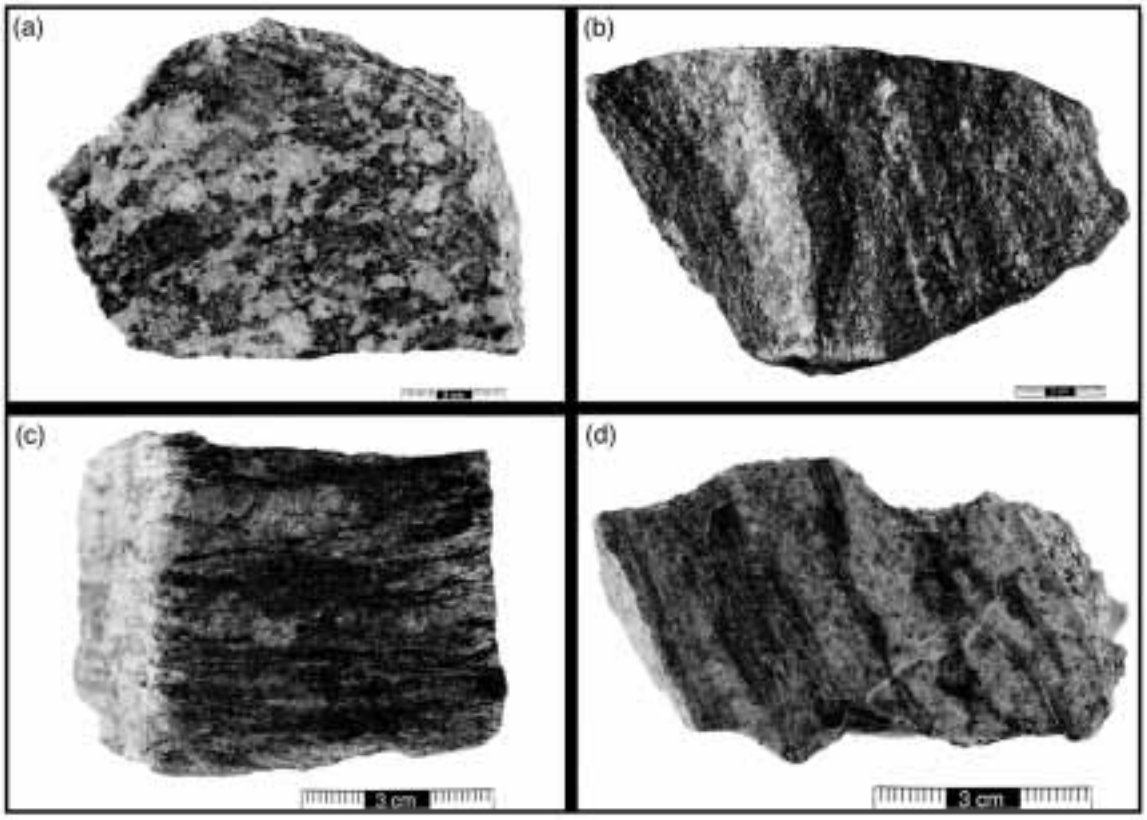

Fig. 3. Photographs of hand specimens of the different migmatite types. (a) MIG1 migmatite with no clear leucosomes and mesosomes, but vaguely distinguishable light and dark areas. The absence of foliation and layering should be noted. (b) MIG2 migmatite with a pronounced layering of mesosomes and leucosomes and a moderately developed foliation. (c) MIG3 migmatite with a weakly developed mesosome–leucosome layering and a pronounced foliation. (d) MIG4 migmatite with a pronounced layering of melanosomes and leucosomes and a strongly developed foliation.

migmatite type (Berger & Kalt, 1999). MIG2 migmatites are characterized by a pronounced interlayering of mesosome with leucosome and by a weakly developed foliation (Fig. 3b). In MIG3 migmatites, foliation is more strongly developed, layering of mesosome and leucosome is less pronounced than in MIG2 migmatites, and leucosome margins with mesosome are usually diffuse (Fig. 3c). MIG4 migmatites are characterized by an interlayering of melanosome and leucosome with sharp margins and display pronounced foliation and stretching lineation (Fig. 3d). Millimetre- to decimetre-sized leucosomes discordant to foliation may occur in MIG2–MIG4 migmatite types.

In the field, the different migmatite types alternate on the scale of decimetres to tens of metres (Fig. 4a–d). The stromatic and foliated MIG3 migmatites are by far the most abundant (Fig. 4b, d). MIG3 migmatites may grade into type MIG2 (Fig. 4a), particularly at sites of strain inhomogeneity such as the borders to lenses or bands of gneisses and calc-silicate rocks. Melanosome-bearing MIG4 migmatites occur as local decimetre-sized bodies or boudins in MIG3 migmatites (Fig. 4b) and may also grade into MIG2 migmatites (Fig. 4c). MIG2–MIG4 migmatites may contain narrow dark selvages of biotite within their leucosomes or at leucosome rims (Fig. 4a, c, d). MIG1 migmatites are comparatively rare and form massive parts of variable size within the stromatic migmatite types (Fig. 4a, c).

PETROGRAPHY

Massive migmatites (MIG1)

Bulk modal compositions of MIG1 migmatites are 16–24% quartz, 39–58% feldspar, 14–16% biotite, 11–22% cordierite and up to 0·5% sillimanite. Main phases in the small light areas are plagioclase, quartz, cordierite and minor perthitic K-feldspar. Cordierite is usually devoid of inclusions (type cI, Fig. 5a). Type cI cordierites and accompanying feldspars are large (1–2 mm) and euhedral. The dark areas contain biotite, cordierite and less quartz and feldspar. Some rocks additionally have

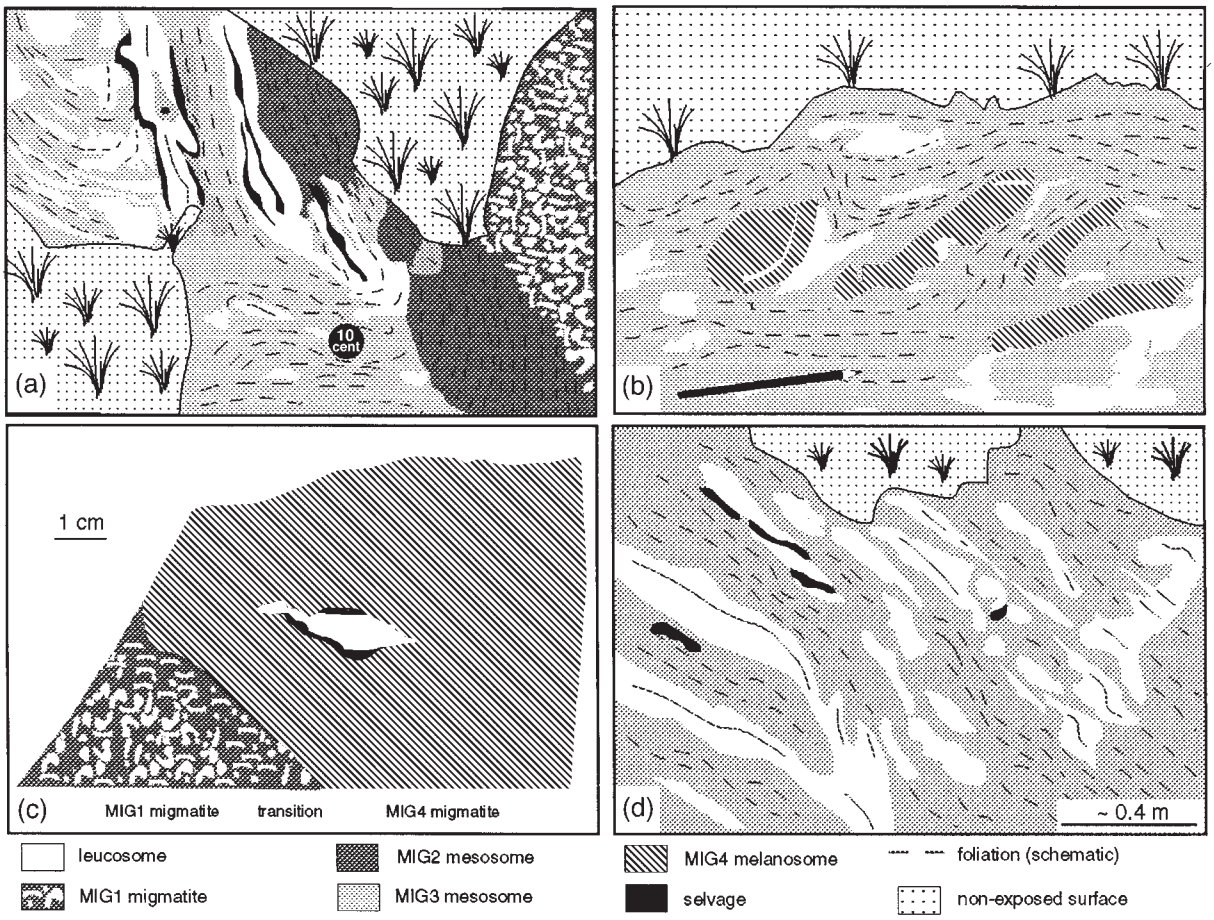

Fig. 4. Schematic drawings of field relationships from photographs, showing the alternation of the different migmatite types on various scales. The signatures are supposed to distinguish migmatite types and to reflect brightness contrasts. The leucosome signature represents both K-feldspar and quartz-dominated leucosomes and plagioclase-bearing leucosomes (see section on petrography). In the signature for MIG4 melanosomes, dashed lines indicate the approximate orientation of foliation. (a) Alternation of MIG1–MIG4 migmatites on the centimetre to decimetre scale. (b) Decimetre-sized bodies of MIG4 melanosomes in an MIG3 migmatite. (c) MIG4 melanosome grading into an MIG1 migmatite in a hand specimen. (d) Typical outcrop of an MIG3 migmatite.

minor garnet in these dark areas. Cordierite is surrounded by blocky biotite laths and commonly displays inclusions of sillimanite needles, in some cases with small grains of biotite and ilmenite (type cII, Fig. 5b). The outermost rims of cII cordierites are always inclusion free (Fig. 5b). Biotite laths adjacent to K-feldspar and cordierite may display embayed or skeletal forms (Fig. 5c) with fine-grained aggregates of feldspars and quartz grown between them (Fig. 5c). Accessory phases are ilmenite, graphite, pyrrhotite and pyrite. In very rare cases, spinel is present as inclusions in garnet and cordierite.

Stromatic migmatites (MIG2)

In MIG2 migmatites, cordierite, biotite, garnet, perthitic K-feldspar, plagioclase and quartz are the most abundant phases. Sillimanite and spinel are present only as inclusions but are more abundant than in MIG1 migmatites. Accessory phases are ilmenite, graphite, pyrrhotite and pyrite.

Modal compositions of mesosomes are 0·5–2·0% quartz, 17–20% feldspar, 30–35% biotite, 40–45% cordierite and up to 2% garnet and sillimanite, respectively. These values indicate a depletion in quartz and feldspars compared with MIG1 compositions. Cordierites are mainly of type cII (Fig. 5b). The mesosomes may contain large to very large hypidioblastic garnets with abundant and diverse inclusions, the most common being quartz, biotite and sillimanite. Very large garnets (up to 6 mm) may display a colour zoning under the microscope, with pink–brown inner cores and lighter pink outer cores and rims (type gI; see Table 1 and section on mineral chemistry). The inner cores have rare tiny inclusions of

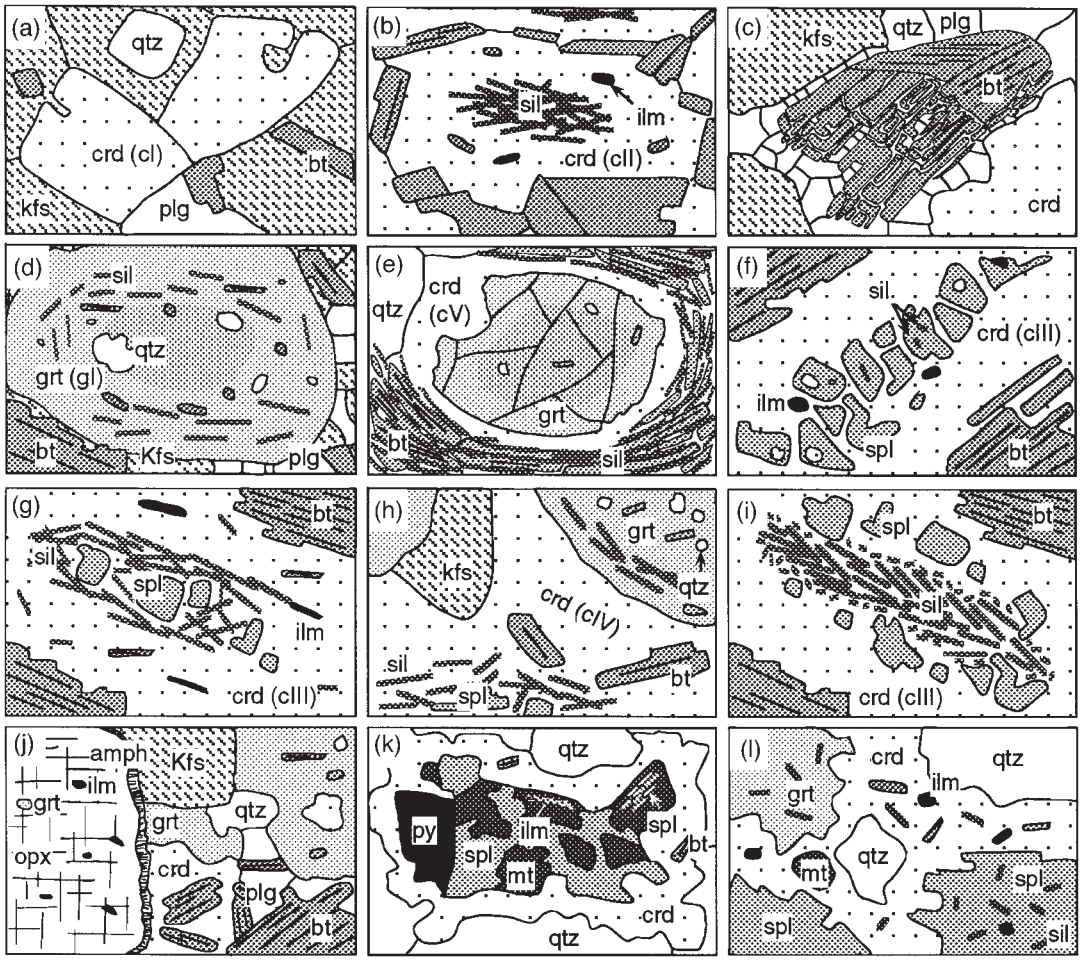

Fig. 5. Schematic drawings of the main textural features of the metapelites from the Bayerische Wald. (a) Subhedral to euhedral blasts of cordierite type cI surrounded by K-feldspar, quartz and plagioclase. (b) Cordierite of type cII, with sillimanite inclusions. (c) Biotite shows embayed and skeletal forms in the lower part of the grain and is intimately intergrown with fine-grained plagioclase, quartz and with K-feldspar. (d) Garnet of type gI. The inner cores are comparatively dark, have rare inclusions and are free of sillimanite, whereas the outer cores are light and display frequent inclusions of sillimanite, biotite and quartz. (e) Cordierite (type cV), forming postkinematically between garnet (type gI) and intergrowths of biotite, sillimanite and quartz. (f) Cordierite of type cIII with spinel and ilmenite inclusions. (Note the sillimanite inclusions in spinel.) (g) Cordierite of type cIII, with additional sillimanite and biotite inclusions. (h) Intergrowth of cordierite (type cIV), garnet, K-feldspar, spinel, quartz and minor biotite. (i) Dense aggregates of sillimanite needles in cII cordierites, perhaps pseudomorphing former kyanite. (j) Coexisting orthopyroxene, garnet, cordierite, K-feldspar and biotite in orthopyroxene-bearing migmatites. Amphibole seams around orthopyroxene are secondary. (k) Intergrowths of magnetite and spinel ± pyrite/pyrrhotite ± ilmenite in magnetite-bearing intercalations. Exsolution lamellae of spinel and ilmenite in magnetite and the continuous grain boundary of magnetite and spinel towards cordierite should be noted. The latter is formed at the expense of a former complex spinel and quartz. (l) Framework of cordierite bordering garnet and spinel, both with sillimanite inclusions.

quartz and various accessory phases (zircon, monazite, in some cases also pyrite, pyrrhotite and rutile) and are always devoid of sillimanite (Fig. 5d). The outer cores commonly display many inclusions of quartz, biotite and sillimanite needles (Fig. 5d), and in some cases also K-feldspar and spinel. Quartz inclusions in a few gI garnets, situated at the border between inner and outer cores, have primary fluid inclusions containing N_2 and secondary fluid inclusions composed of CO_2. Large garnets (1–3 mm, type gII) correspond to the outer cores of type gI garnets in terms of colour, inclusion relations and composition (see Table 1 and section on mineral chemistry).

Most of the leucosomes in MIG2 migmatites consist of K-feldspar, plagioclase and quartz. In rare cases, K-feldspar and quartz-dominated leucosomes were observed. Plagioclase-bearing leucosomes may contain cordierite (cI), garnet and biotite. Garnets are usually smaller than in mesosomes, idioblastic to rounded and largely free of inclusions except for rare zircon, monazite, pyrite, pyrrhotite and quartz (type gIII; see Table 1).

Table 1: Textures and phase assemblages of the samples

Sample	Type		Phases										
			Crd, type	Grt, type	Bt	Spl	Ilm	Sil	Pl	Kfs	Qtz	Opx	Cpx
BW-06	MIG1		cI–cII	—	+	—	+	ic	+	+	+	–	–
BW-13a	MIG4		cI–cIII	gII	+	ic	+	icgs	+	+	+	–	–
BW-13c	MIG4		cI–cIII	gI–gII	+	ic	+	ics	+	+	+	–	–
BW-18	MIG3/4		cI–cIV	gII	+	ic	+	ic	+	+	+	–	–
BW-19	MIG1		cI–cIII	gI–gII	+	icg	+	icg	+	+	+	–	–
BW-28	MIG2		cI–cIII	gII	+	ic	+	icg	+	+	+	–	–
BW-29	MIG3		cI–cIII, (cV)	gI–gII	+	icb	+	ic	+	+	+	–	–
BW-34	MIG3	L	cI	gII–gIII	+	—	+	—	+	+	+	–	–
BW-36	MIG3		cI–cII	gIII	+	—	+	—	+	+	+	–	–
BW-44	MIG3/1	L	—	gI, gIII	+	—	—	—	+	+	+	–	–
	MIG3/1	MS	cI–II	gI, gIII	+	—	+	ic	+	+	+	–	–
BW-45	MIG1		cI–cII	gII	+	—	+	ic	+	+	+	–	–
BW-46	MIG1		cI–cIII	gI–gII	+	ic	+	icg	+	+	+	–	–
BW-66	MIG1/4		cI–cII	gII	+	—	+	—	+	+	+	–	–
BW-81	MIG3		cI–cIII	gII	+	ic	+	icg	+	+	+	–	–
BW-83	MIG4		cI–cIV	gII	+	ic	+	icgs	+	+	+	–	–
BM-01	MIG4	L	cI	—	+	—	—	—	(+)	+	+	–	–
	MIG4	ML	cI–cIV, (cV)	gI–gII	+	ic	+	icgb	+	+	+	–	–
E-22	MIG3	L	cI	—	+	—	—	—	+	+	+	–	–
	MIG3	M	cI–cV	gI–gII	+	ic	+	icgb	+	+	+	–	–
BW-20	MR		+	+	+	+	+	igcbs	+	—	+	–	–
86246	MR		+	+	+	+	+	—	+	+	+	–	–
BL-1	OM		+	+	+	—	+	—	+	+	+	+	–
BW-39	G		—	—	+	—	+	—	+	—	+	+	+

Mineral abbreviations according to Kretz (1983); MIG1–MIG4, migmatite types (whole rock); MR, magnetite-bearing rock; OM, orthopyroxene-bearing migmatite; G, mafic granulite; L, leucosome; MS, mesosome; ML, melanosome; +, major or minor phase; —, not present; ib, included in biotite; ic, included in cordierite; ig, included in garnet, is, included in spinel. Accessory apatite, zircon, monazite, graphite, pyrrhotite and xenotime are common in most samples. Samples BW-39 and BL-1 additionally contain secondary amphibole. Secondary muscovite is present in samples BW-66, E-22M and E-22L. (For further explanation, see section on petrography.)

Foliated stromatic migmatites (MIG3)

Modal compositions of MIG3 mesosomes are similar to the MIG1 compositions, indicating no or only minor depletion in quartz and feldspar when compared with the latter. The samples contain cordierite (14–22%), biotite (15–24%), quartz (18–22%), feldspar (34–36%), garnet (0–6%), sillimanite (0–10%), ilmenite and in some cases accessory graphite, pyrrhotite and pyrite in their mesosomes. Sillimanite is usually present as inclusions in cordierite and garnet (gI outer cores, gII) and is very rarely also intergrown with biotite (Fig. 5e). Spinel, when present, forms inclusions in cordierite. Garnets are of types gI and gII. Cordierites are mainly of type cI (Fig. 5a) and cII (Fig. 5b). Biotite often displays the aforementioned embayed or skeletal forms (Fig. 5c). Leucosomes in MIG3 migmatites are mainly of the K-feldspar- and quartz-dominated type.

Melanosome-bearing migmatites (MIG4)

The melanosomes of MIG4 migmatites have modal compositions similar to those present as solid phase assemblages during dehydration melting experiments (e.g. Le Breton & Thompson, 1988; Vielzeuf & Holloway, 1988; Patiño Douce & Johnston, 1991; Skjerlie & Johnston, 1993; Vielzeuf & Montel, 1994; Carrington & Harley, 1995). They consist of biotite (4–22%), garnet (2–5%), cordierite (52–57%), sillimanite (2–22%), spinel, ilmenite and accessory graphite, pyrrhotite and pyrite, and are strongly depleted in quartz (0–3%) and feldspars (13–15%) compared with MIG1 compositions.

In MIG4 melanosomes, garnet always forms large elongate grains which are of type gI and gII (see Table 1 and section on mineral chemistry). Most cordierite is surrounded by biotite laths and has inclusions of sillimanite and/or spinel ± ilmenite ± biotite ± garnet.

Most abundant are cordierites of type cIII in which spinel forms elongate skeletal aggregates of small embayed grains that may have tiny sillimanite and biotite inclusions (Fig. 5f). Needles of sillimanite and small laths of ilmenite and biotite may additionally be present in cIII cordierites (Fig. 5g) and their outermost rims are always devoid of inclusions (Figs. 3f, g). Type cII cordierites (Fig. 5b) are also present. Some large cordierite blasts are intergrown with garnet, biotite, K-feldspar, spinel and sillimanite (type cIV, Fig. 5h). In a few samples, thin postkinematic seams of cordierite have grown at the expense of large garnet grains (type cV, Fig. 5e). These seams may broaden to larger blasts and replace garnet entirely in some cases.

Sillimanite is restricted to inclusions in cordierite, spinel, garnet (gI outer cores, gII) and is intergrown with biotite and quartz in very few cases (Fig. 5e). In some cordierites, aggregates of sillimanite seem to pseudomorph larger blades or laths, perhaps former kyanite (Fig 5i). Sillimanite may form prismatic crystals and is much more abundant than in MIG1 and MIG2 migmatites. MIG4 melanosomes are generally associated with K-feldspar and quartz-dominated leucosomes. Very rarely, plagioclase-bearing leucosomes occur.

Intercalations in MIG2 and MIG3 migmatites

Orthopyroxene-bearing migmatites

Migmatites with orthopyroxene form rare decimetre-sized bands and lenses in MIG2 and MIG3 migmatites that can be traced along the strike of migmatite foliation from south of Cham to north of Viechtach (Fig. 2). Textures within these intercalations are very irregular, with foliation being largely absent and leucosomes and mesosomes not clearly separated. The rocks are composed of large orthopyroxene and garnet grains surrounded by smaller cordierite, K-feldspar, plagioclase, quartz and biotite grains (Fig. 5j) and accessory ilmenite, graphite and pyrite. Orthopyroxene forms large hypidioblastic grains with rare inclusions of garnet and ilmenite. Garnets are hypidioblastic to xenoblastic and have inclusions of biotite, quartz, ilmenite and cordierite. The last also forms isolated grains that lack inclusions and are surrounded by feldspars, quartz and biotite. Biotite laths may show features as displayed in Fig. 5c. Secondary coronas of amphibole are present around orthopyroxene.

Magnetite-bearing rocks

These rocks occur as bands and lenses within MIG2 and MIG3 migmatites in the immediate vicinity of the Silberberg sulphide ore deposit near Bodenmais (Fig. 2). Formation of the pyrrhotite–pyrite–magnetite–sphalerite assemblage in the ore deposit itself was concurrent with peak metamorphism and partial melting in the surrounding migmatites (Schreyer *et al.*, 1964).

Most of the magnetite-bearing rocks have gneissose textures. The largest grains are garnets with inclusions of quartz, sillimanite and rare spinel and biotite. Of approximately the same size are aggregates of spinel $\pm$ magnetite $\pm$ ilmenite which may be intergrown with pyrrhotite and/or pyrite (Fig. 5k). Spinel is mainly located at the rims of magnetite with lobate grain boundaries towards the latter as described by Waters (1991), but may also occur as exsolved spindles in magnetite (Fig. 5k). Larger spinel grains may have inclusions of sillimanite and rare biotite. Ilmenite forms bands of blebs and spindles in magnetite (Fig. 5k). Garnets and the oxide–sulphide intergrowths are surrounded by quartz and plagioclase. Quartz and spinel are separated by thin rims of cordierite. The latter may also form between garnet and spinel. The two types of cordierite rims may intergrow to form a framework (Fig. 5l). Biotite is very rare and may occur as inclusions in garnet, spinel and cordierite. K-feldspar is absent.

Amphibolitized mafic granulites

Mafic granulites can be found as lenses or loose blocks within migmatites of types MIG1, MIG2 and MIG3. They are dense, fine-grained, massive to weakly foliated rocks with heterogranular textures. Clinopyroxene and orthopyroxene form the largest grains. At their rims, clinoamphibole and orthoamphibole, respectively, form and may replace the pyroxenes to different degrees. Plagioclase and quartz form smaller grains. Small apatite and ilmenite grains are very abundant, and biotite and zircon are accessory phases.

PARTIAL MELTING

A number of observations and considerations require that in migmatites melt was produced, segregated to different degrees and crystallized mainly in leucosomes:

(1) The presence of discordant leucosomes that are not related to granites requires production and segregation of melt.

(2) In strongly layered MIG2 and MIG4 migmatites, leucosome compositions and microstructures (Berger & Kalt, 1999), quartz and feldspar depletion in mesosomes and the restitic character of some melanosomes point to melt extraction from meso- and melanosomes and segregation into concordant leucosomes.

(3) In mesosomes that are relatively undepleted in quartz and feldspar (MIG1 and MIG3), melt-controlled crystallization is indicated by cordierite and biotite fabrics (Berger & Kalt, 1999).

(4) The main mineral assemblages and reaction textures reflect the dehydration melting reactions that have been

derived from grids and obtained from dehydration experiments for similar bulk compositions (see section on mineral reactions).

(5) Although metamorphic conditions cannot be precisely quantified, semiquantitative estimates of peak conditions and thermobarometric calculations for retrograde stage D (see sections on mineral assemblages and thermobarometry) indicate that temperatures were above those required for dehydration melting in compositionally similar experimental systems, even in the absence of an aqueous fluid (see section on quantitative *P–T* constraints). Hence, melting must have taken place.

(6) H_2O and CO_2 contents of cordierite suggest equilibration with a peraluminous H_2O-undersaturated melt rather than with an aqueous or carbonic fluid [Kalt (unpublished data) and section on fluids].

In magnetite-bearing rocks and in mafic granulites there is no indication for melting.

MINERAL ASSEMBLAGES

On the basis of textures and inclusion relations, mineral assemblages observed in MIG1–MIG4 migmatites and their intercalations can be divided into four generations, indicating four metamorphic stages. No textural characteristics of stage A are preserved. Stages B and C are clearly concurrent with foliation (synkinematic), and stage D is postkinematic.

Stage A

Stage A is only recorded in mesosomes and melanosomes of MIG2–MIG4 migmatites by the sillimanite-free, dark inner cores of the very large gI garnets. The relic assemblage is garnet (grt) + quartz (qtz).

Stage B

A number of assemblages developed simultaneously with foliation in the different migmatite domains: mesosome (MIG1–MIG3), biotite (bt) + cordierite (crd) + K-feldspar (Kfs) + plagioclase (plg) + (qtz) ± sillimanite (sil) ± (grt) ± spinel (spl); melanosome (MIG4), bt + crd + sil + grt + spl ± Kfs ± plg ± qtz; orthopyroxene-bearing migmatites, orthopyroxene (opx) + grt + crd + bt + qtz + plg; magnetite-bearing rocks, grt + sil + qtz + composite spinel (spl_{ss}) + plg ± bt; mafic granulites, opx + clinopyroxene (cpx) + plg + qtz. The garnet types stable at stage B in MIG1–MIG4 migmatites are gI (except the inner cores), gII and gIII, with the outermost rims of all garnet types being modified later by diffusion and/or resorption (see section on mineral chemistry). The cordierite types stable in MIG1–MIG4 migmatites at stage B are cI–cIV. Analysis of stage B reactions and the evidence for partial melting outlined above indicate that melt formed with stage B mineral assemblages.

Stage C

In MIG1 migmatites and in MIG2–MIG4 mesosomes and melanosomes, stage C is characterized by the same assemblages as stage B. The melt produced at stage B crystallizes and forms two assemblages in leucosomes of MIG2–MIG4 migmatites: Kfs + qtz and Kfs + qtz + plg ± crd ± grt ± bt.

Stage D

Postkinematic stage D assemblages are grt + crd + sil + qtz in some MIG2–MIG4 migmatites (cV, Fig. 5e) and crd + spl_{ss} + qtz in magnetite-bearing rocks (Fig. 5k).

After stage D, migmatites and their intercalations were in part affected by minor retrograde hydration. Formation of amphiboles at the expense of pyroxenes in granulites and thin coronas of amphibole around orthopyroxene in migmatites (Fig. 5j) took place under amphibolite-facies conditions. Formation of pinite from cordierite along rims and cracks, formation of muscovite and chlorite from biotite and sericitization of plagioclase occurred even later under greenschist-facies conditions.

MINERAL CHEMISTRY

Analytical techniques

Microprobe analyses were performed using a Cameca SX 51 microprobe equipped with five wavelength-dispersive spectrometers. Operating conditions were 20 nA beam current, 15 kV accelerating voltage, 10 s counting time for all elements except Ti in spinel (30 s), Mg, Ca and Al in spinel (20 s), and Zn in spinel and cordierite (40 s). PAP correction was applied to the data. Natural and synthetic oxide and silicate standards were used for calibration.

For Na-in-cordierite thermometry between 41 and 370 cordierite analyses per sample were performed (see Kalt *et al.*, 1998). The detection limit for Na in natural oxide and silicate standards is 0·049 wt % employing operating conditions as detailed above. Under these conditions the precision of Na measurements ($n = 20$) is 0·10 ± 0·01 wt % (0·007 ± 0·001 c.p.f.u.) on a diopside standard, 1·32 ± 0·04 wt % (0·094 ± 0·003 c.p.f.u.) on an augite standard, 0·85 ± 0·003 wt % (0·060 ± 0·002 c.p.f.u.) on a Cr-augite standard, and 0·12 ± 0·02 wt % (0·018

Table 2: Compositional ranges of the main phases

Sample	X_{Mg} (Crd)	X_{Mg} (Bt)	X_{Mg} (Spl)	X_{Mg} (Grt)	An (Pl)
BW-06	0·524–0·549	0·367–0·430	—	—	0·141–0·244
BW-13a	0·567–0·610	0·406–0·488	0·109–0·141	0·161–0·218	0·218–0·273
BW-13c	0·565–0·607	0·402–0·491	0·108–0·131	0·167–0·225	0·207–0·284
BW-18	0·639–0·708	0·467–0·535	0·086–0·100	0·190–0·232	0·290–0·356
BW-19	0·635–0·681	0·471–0·495	0·189–0·202	0·132–0·254	0·346–0·422
BW-28	0·552–0·589	0·387–0·430	0·038–0·057	0·100–0·122	0·236–0·256
BW-29	0·405–0·438	0·355–0·399	0·021–0·026	0·080–0·148	n.d.
BW-34	0·482–0·517	0·358–0·378	—	0·116–0·145	0·253–0·278
BW-36	0·623–0·644	0·458–0·519	—	0·154–0·234	0·290–0·339
BW-44L	—	0·428–0·459	—	0·010–0·221	0·238–0·254
BW-44M	0·549–0·589	0·395–0·439	—	0·095–0·178	0·237–0·293
BW-45	0·543–0·596	0·383–0·436	—	0·082–0·190	0·248–0·301
BW-46	0·541–0·581	0·359–0·383	0·128–0·204	0·086–0·191	0·270–0·308
BW-66	0·619–0·639	0·462–0·495	—	0·210–0·235	0·264–0·298
BW-81	0·605–0·649	0·468–0·490	0·102–0·130	0·183–0·268	0·244–0·282
BW-83	0·531–0·576	0·445–0·489	0·043–0·052	0·135–0·182	0·240–0·341
BM-01L	0·469–0·498	0·248–0·265	—	—	n.d.
BM-01M	0·472–0·558	0·245–0·268	—	0·081–0·193	n.d.
E-22L	0·438–0·501	0·310–0·351	—	—	0·275–0·395
E-22M	0·432–0·518	0·327–0·355	—	0·058–0·104	0·344–0·405
BW-20	0·488–0·545	0·395–0·489	0·020–0·027	0·115–0·146	n.d.
86246	0·622–0·672	n.d.	0·034–0·038	0·132–0·271	0·851–0·998
BL-1	0·721–0·744	0·519–0·530	—	0·261–0·312	n.d.

Mineral abbreviations according to Kretz (1983). X_{Mg} = Mg/(Mg + Fe), except for garnet where X_{Mg} = Mg/(Mg + Fe + Mn + Ca).

± 0·002 c.p.f.u.) on a garnet standard. In all measurements, Na and K were analysed as the first elements to avoid volatilization. Measurements with defocused beam or longer counting times at lower beam current did not change these values.

Compositional ranges of major phases in all samples are indicated in Table 2. Garnet and cordierite compositions are listed in Table 3 and Table 4, respectively. Additionally, selected mineral analyses are presented in Table 5.

Phase compositions

Garnet

In MIG1–MIG4 migmatites, garnets are very Fe rich, with X_{Mg} values [X_{Mg} = Mg/(Mg + Fe + Ca + Mn)] of 0·058–0·268, MnO contents of 0·1–6·5 wt %, and CaO contents between 0·7 and 4·3 wt % (Table 3). All garnet types display distinct zoning patterns and inclusion relations (see section on petrography). Type gI garnets show inner cores characterized by comparatively high CaO and MnO contents decreasing outward, very low MgO contents increasing outward, and very high FeO contents that slightly increase outward (Fig. 6a). The outer cores of gI garnets display lower MnO and CaO contents and higher MgO and FeO contents compared with the inner cores (Fig. 6a). At the outermost rims of gI garnets increasing MnO and FeO contents as well as decreasing MgO contents can be observed (Fig. 6a).

Type gII garnets are smaller and show a simple zoning pattern similar to the zoning in outer cores and rims of type I garnets (Fig. 6b). MgO and CaO decrease outward whereas FeO and MnO increase outward. The comparatively small grainsize of gII garnets and their compositional similarity to gI garnet outer cores suggest that both garnet domains were formed at the same time. Type gIII garnets show constant FeO, MnO, CaO and MnO concentrations in their cores as well as increasing FeO and decreasing MgO contents at their outermost rims. Comparison of compositions reveals that gIII garnets probably grew at the same time as the cores of gII garnets and the outer cores of gI garnets. GI and gII garnets occur in mesosomes and were thus subject to

Table 3: Selected garnet compositions

	BW-29 gI ic	BW-29 gI oc	BW-29 gI rim	BW-13a gII core	BW-18 gII core	BW-18 gII rim	BW-34 gIII core	BW-34 gIII rim	86246 core	BL-1 core
SiO_2	36·94	37·08	36·85	37·52	37·97	37·65	37·28	36·98	37·40	38·48
TiO_2	0·05	0·05	0·03	0·01	0·01	0·02	0·02	0·00	0·05	0·01
Al_2O_3	20·31	20·47	20·61	21·15	21·22	21·19	20·85	20·67	20·78	21·42
Cr_2O_3	0·00	0·02	0·02	0·03	0·01	0·00	0·04	0·02	0·00	0·03
Fe_2O_3	n.d.	n.d.	n.d.	n.d.	n.d.	n.d.	n.d.	n.d.	n.d.	n.d.
FeO	32·37	36·11	37·67	33·51	32·24	33·85	34·83	35·74	36·03	29·89
MnO	4·08	1·84	1·93	1·33	1·26	1·61	2·45	2·77	0·03	1·32
MgO	1·98	3·17	2·00	5·62	5·98	4·87	3·67	2·92	4·16	7·67
CaO	4·28	1·25	1·03	0·86	1·35	1·24	0·95	0·97	2·11	1·19
Na_2O	0·00	0·00	0·02	0·01	0·03	0·00	0·01	0·01	0·00	0·00
K_2O	0·00	0·01	0·01	0·00	0·00	0·00	0·00	0·02	0·00	0·00
Total	100·01	100·00	100·17	100·04	100·07	100·43	100·10	100·10	100·56	100·01
Si	2·998	3·001	2·999	2·983	3·000	2·991	2·998	2·995	2·987	3·004
Ti	0·003	0·003	0·002	0·000	0·001	0·001	0·001	0·000	0·003	0·001
Al	1·943	1·953	1·977	1·982	1·976	1·985	1·976	1·973	1·957	1·971
Cr	0·000	0·001	0·001	0·002	0·001	0·000	0·002	0·001	0·000	0·002
Fe^{3+}	n.c.	n.c.	n.c.	n.c.	n.c.	n.c.	n.c.	n.c.	n.c.	n.c.
Fe^{2+}	2·191	2·444	2·565	2·228	2·130	2·249	2·343	2·421	2·407	1·952
Mn	0·280	0·126	0·133	0·090	0·085	0·108	0·167	0·190	0·002	0·087
Mg	0·240	0·382	0·243	0·667	0·704	0·576	0·440	0·352	0·495	0·892
Ca	0·372	0·109	0·090	0·073	0·114	0·105	0·082	0·084	0·180	0·099
Na	0·000	0·000	0·003	0·001	0·004	0·000	0·002	0·001	0·000	0·000
K	0·000	0·001	0·001	0·000	0·000	0·000	0·000	0·002	0·001	0·000
Total	8·027	8·020	8·014	8·026	8·015	8·015	8·011	8·019	8·032	8·008

Formula calculations on the basis of 12 oxygens. n.d., not determined; n.c., not calculated; gI–gIII, garnet types; ic, inner core; oc, outer core. (For explanation, see Fig. 6 and section on phase compositions.) Garnets contain no Zn.

Table 4: Selected cordierite core compositions

	BW-06	BL-1	BW-13c	BW-18	BW-20	BW-29	BW-34	BW-36	BM-01M	BM-01L
SiO_2	48·50	48·98	48·80	48·71	47·52	47·50	47·82	48·96	47·86	47·90
TiO_2	0·01	0·00	0·00	0·00	0·02	0·00	0·00	0·00	0·00	0·00
Al_2O_3	31·98	32·69	32·61	32·51	32·30	31·99	31·91	32·48	32·49	32·50
Cr_2O_3	0·00	0·00	0·00	0·00	0·00	0·00	0·00	0·00	0·00	0·00
Fe_2O_3	n.d.	n.d.	n.d.	n.d.	n.d.	n.d.	n.d.	n.d.	n.d.	n.d.
FeO	11·10	6·57	9·64	7·97	11·62	13·64	11·28	8·66	10·22	11·83
MnO	0·24	0·09	0·13	0·13	0·25	0·29	0·25	0·21	0·15	0·15
MgO	6·92	9·65	7·89	8·56	6·67	5·58	6·68	8·14	7·16	6·10
CaO	0·01	0·02	0·02	0·04	0·03	0·02	0·00	0·01	0·03	0·02
Na_2O	0·15	0·14	0·12	0·10	0·05	0·12	0·13	0·09	0·12	0·11
K_2O	0·00	0·01	0·01	0·00	0·00	0·00	0·00	0·00	0·00	0·01
ZnO	0·00	0·00	0·00	0·00	0·00	0·00	0·00	0·00	0·00	0·00
H_2O	n.d.	n.d.	n.d.	n.d.	n.d.	n.d.	n.d.	n.d.	n.d.	n.d.
Total	98·91	98·15	99·22	98·02	98·46	99·14	98·07	98·55	98·03	98·62
Si	5·032	5·013	5·010	5·022	4·969	4·981	5·011	5·036	4·990	4·998
Ti	0·001	0·000	0·000	0·000	0·002	0·000	0·000	0·000	0·000	0·000
Al	3·910	3·943	3·946	3·951	3·980	3·953	3·941	3·938	3·992	3·997
Cr	0·000	0·000	0·000	0·000	0·000	0·000	0·000	0·000	0·000	0·000
Fe^{3+}	n.c.	n.c.	n.c.	n.c.	n.c.	n.c.	n.c.	n.c.	n.c.	n.c.
Fe^{2+}	0·963	0·562	0·828	0·687	1·016	1·196	0·989	0·745	0·891	1·032
Mn	0·021	0·008	0·011	0·012	0·022	0·025	0·023	0·018	0·013	0·013
Mg	1·071	1·472	1·207	1·316	1·040	0·872	1·043	1·248	1·113	0·948
Ca	0·001	0·002	0·002	0·004	0·004	0·002	0·000	0·001	0·003	0·002
Na	0·031	0·029	0·023	0·019	0·011	0·024	0·026	0·018	0·024	0·022
K	0·000	0·001	0·000	0·000	0·000	0·000	0·000	0·000	0·000	0·002
Zn	0·000	0·000	0·000	0·000	0·000	0·000	0·000	0·000	0·000	0·000
H_2O	n.c.	n.c.	n.c.	n.c.	n.c.	n.c.	n.c.	n.c.	n.c.	n.c.
Total	11·030	11·030	11·027	11·011	11·044	11·053	11·033	11·004	11·026	11·014

Formula calculations on the basis of 18 oxygens. n.d., not determined; n.c., not calculated.

Fe–Mg–Mn exchange with biotite and cordierite, resulting in the observed zoning patterns. GIII garnets occur in leucosomes. They do not display significant zoning because of the scarcity of Fe–Mg phases in leucosomes. Some larger gIII garnets show very small cores with elevated MnO and CaO contents, comparable with the inner cores of gI garnets. This suggests the presence of a few gI inner cores as nucleation sites in the leucosomes.

In orthopyroxene-bearing migmatites (sample BL-1), garnets have X_{Mg} values of 0·261–0·312, Mn contents of 1·1–1·5 wt %, and CaO contents of 1·1–1·2 wt % (Table 3). Garnets are unzoned except for a minor decrease in MgO and increase in FeO and MnO contents at the outermost rims. Garnets in magnetite-bearing rocks are also homogeneous except for their outermost rims. X_{Mg} values range from 0·12 to 0·24, CaO contents from 1·4 to 3·2 wt % and MnO contents from 0·12 to 0·29 wt %.

Cordierite

Within individual MIG1–MIG4 migmatite samples cordierite compositions are fairly homogeneous (Table 4; Fig. 7) and there is no systematic compositional difference among the different textural cordierite types (cI–cIV; see section on petrography). From cores to rims cordierite grains have constant Al/(Al + Si) values and Na_2O and MnO contents but may show minor variations in X_{Mg} [X_{Mg} = Mg/(Mg + Fe), Fig. 7a]. Comparing cordierites from different samples the largest variations occur in X_{Mg} (0·405–0·708), Na_2O (0·05–0·21 wt %) and MnO (0·11–0·36 wt %). Zn contents of all cordierites are below detection limit (0·02 wt %). Cordierites of a few samples were checked for Li, Be, B and P by secondary ion mass spectrometry and were found to contain only minor amounts of these elements (Li: 18–133 ppm; Be: 1–49 ppm; B: 1–8 ppm; P: 35–113 ppm). H_2O (0·21–0·75 wt %) and 0·04–0·16 wt % CO_2 were measured in the

Table 5: Selected mineral compositions

	BW-06	BW-13a			BW-18			BW-20		
	Bt	Bt	Kfs	Spl	Bt	Plg	Spl	Bt	Ilm	Spl
SiO_2	35·05	35·02	64·17	0·01	35·35	59·65	0·00	35·28	0·02	0·00
TiO_2	4·15	3·85	0·00	0·02	4·00	0·00	0·02	4·09	51·90	0·06
Al_2O_3	18·76	17·90	19·13	57·86	18·31	26·04	59·01	17·06	0·00	53·90
Cr_2O_3	0·08	0·11	0·00	0·69	0·00	0·00	0·03	0·02	0·01	0·03
Fe_2O_3	n.d.	n.d.	0·21	1·25	n.d.	0·07	1·65	n.d.	n.d.	6·42
FeO	21·01	20·90	0·00	33·30	17·52	0·00	32·83	21·99	46·03	36·15
MnO	0·08	0·09	0·00	0·16	0·11	0·00	0·19	0·04	1·12	0·35
MgO	7·05	8·12	0·00	2·92	10·90	0·00	4·59	7·98	0·11	1·85
CaO	0·00	0·00	0·00	0·01	0·00	7·20	0·03	0·00	0·01	0·02
Na_2O	0·14	0·09	1·28	0·00	0·29	7·83	0·01	0·14	0·00	0·02
K_2O	9·35	9·57	14·57	0·01	9·19	0·17	0·00	9·29	0·01	0·01
ZnO	0·00	0·00	n.d.	3·52	0·00	n.d.	1·18	0·00	0·00	1·25
H_2O	3·92	3·91	n.d.	n.d.	3·99	n.d.	n.d.	3·91	n.d.	n.d.
Total	99·59	99·56	99·36	99·75	99·66	100·96	99·54	99·80	99·21	100·06
Si	2·680	2·685	2·969	0·000	2·659	2·639	0·000	2·709	0·000	0·000
Ti	0·239	0·222	0·000	0·001	0·226	0·000	0·001	0·236	0·995	0·003
Al	1·691	1·618	1·043	1·955	1·623	1·358	1·158	1·544	0·000	1·855
Cr	0·005	0·006	0·000	0·016	0·000	0·000	0·001	0·001	0·000	0·001
Fe^{3+}	n.c.	n.c.	0·007	0·027	n.c.	0·002	0·021	n.c.	n.c.	0·139
Fe^{2+}	1·344	1·340	0·000	0·798	1·102	0·000	0·457	1·412	0·981	0·883
Mn	0·005	0·006	0·000	0·004	0·007	0·000	0·003	0·003	0·024	0·009
Mg	0·803	0·928	0·000	0·125	1·222	0·000	0·114	0·914	0·004	0·081
Ca	0·000	0·000	0·000	0·000	0·000	0·341	0·001	0·000	0·000	0·001
Na	0·021	0·013	0·115	0·000	0·042	0·672	0·000	0·021	0·000	0·001
K	0·912	0·936	0·860	0·000	0·882	0·010	0·000	0·909	0·000	0·000
Zn	0·000	0·000	n.c.	0·074	0·000	n.c.	0·014	0·000	0·000	0·027
H_2O	2·000	2·000	n.c.	n.c.	2·000	n.c.	n.c.	2·000	n.c.	n.c.
Total	7·700	7·754	4·994	3·000	7·763	5·022	3·000	7·749	2·004	3·000

cordierite channels by *in situ* IR spectroscopy (Kalt, unpublished data). N_2 was detected in some cordierite channels by Raman spectroscopy.

In orthopyroxene-bearing migmatites (sample BL-1), cordierites have X_{Mg} of 0·721–0·744, Na_2O contents of 0·12–0·22 wt % and MnO contents below 0·1 wt % (Table 4). The compositions of cordierites in magnetite-bearing rocks (Table 4) correspond to those in MIG1–MIG4 migmatites.

Biotite

Biotite is a major phase in all samples and is comparatively Fe rich. X_{Mg} values [X_{Mg} = Mg/(Mg + Fe)], range from 0·245 to 0·495 in MIG1–MIG4 migmatites, the differences being greater among than within samples. TiO_2 contents of biotites are between 2·3 and 5·2 wt %, the intra-sample variations being smaller than the inter-sample variation. Single biotite grains are homogeneous except for X_{Mg} values and TiO_2 contents. Both variables may show irregular changes within single grains. The compositions of biotites in magnetite-bearing rocks (Table 4) are similar, whereas biotites in orthopyroxene-bearing migmatites are more magnesian (X_{Mg} of 0·519–0·530) and have TiO_2 contents between 4·2 and 4·8 wt %.

Pyroxenes

In migmatites, orthopyroxenes have X_{Mg} values [X_{Mg} = Mg/(Mg + Fe)] between 0·515 and 0·524, and Al_2O_3 contents of 3·50–3·87 wt %. They are unzoned except for the outermost rims, which have slightly lower X_{Mg} values. In mafic granulites, orthopyroxenes are lower in X_{Mg} (0·473–0·483) and Al_2O_3 (0·39–0·50 wt %). Clinopyroxenes in these rocks have X_{Mg} values of 0·610–0·627 and Al_2O_3 contents of 1·02–1·36 wt %. Both pyroxenes are unzoned.

	BW-34		BW-46			BW-66		BL-1	BW-39	
	Bt	Plg	Bt	Ilm	Spl	Bt	Plg	Opx	Opx	Cpx
SiO_2	34·80	61·43	34·64	0·00	0·01	35·57	61·65	49·75	50·90	52·17
TiO_2	2·97	0·00	4·07	52·43	0·03	4·71	0·00	0·15	0·15	0·25
Al_2O_3	19·18	25·15	18·18	0·00	57·70	16·16	24·77	3·72	0·46	0·73
Cr_2O_3	0·08	0·00	0·10	0·01	0·52	0·01	0·00	0·00	0·04	0·06
Fe_2O_3	n.d.	0·00	n.d.	0·00	1·71	n.d.	0·08	n.d.	n.d.	n.d.
FeO	22·01	0·00	21·61	46·17	32·35	20·18	0·00	28·18	31·07	12·48
MnO	0·14	0·00	0·11	0·51	0·11	0·05	00·0	0·57	0·51	0·29
MgO	7·16	0·00	7·25	0·16	2·42	9·30	0·00	17·20	15·54	11·89
CaO	0·00	5·62	0·00	0·00	0·01	0·00	5·73	0·18	1·05	21·97
Na_2O	0·20	8·53	0·18	0·02	0·11	0·08	8·40	0·00	0·02	0·14
K_2O	9·09	0·26	9·26	0·02	0·00	9·15	0·31	0·00	0·00	0·00
ZnO	0·00	n.d.	0·00	0·00	4·80	0·00	n.d.	n.d.	n.d.	n.d.
H_2O	3·91	n.d.	3·89	n.d.	n.d.	3·91	n.d.	n.d.	n.d.	n.d.
Total	99·54	100·99	99·29	99·32	99·77	99·12	100·94	99·75	99·74	99·98
Si	2·672	2·703	2·670	0·00	0·000	2·726	2·715	1·911	1·988	1·979
Ti	0·172	0·000	0·236	1·001	0·001	0·272	0·000	0·004	0·004	0·007
Al	1·735	1·304	1·651	0·000	1·956	1·460	1·286	0·169	0·021	0·033
Cr	0·005	0·000	0·006	0·000	0·012	0·000	0·000	0·000	0·001	0·002
Fe^{3+}	n.c.	0·000	n.c.	0·000	0·037	n.c.	0·003	n.c.	n.c.	n.c.
Fe^{2+}	1·413	0·000	1·393	0·980	0·778	1·294	0·000	0·905	1·015	0·396
Mn	0·009	0·000	0·007	0·011	0·003	0·003	0·000	0·018	0·017	0·009
Mg	0·820	0·000	0·833	0·006	0·104	1·063	0·000	0·985	0·905	0·672
Ca	0·000	0·265	0·000	0·000	0·000	0·000	0·270	0·007	0·044	0·893
Na	0·030	0·728	0·027	0·001	0·006	0·012	0·717	0·000	0·002	0·010
K	0·890	0·015	0·911	0·001	0·000	0·895	0·018	0·000	0·000	0·000
Zn	0·000	n.c.	0·000	0·000	0·102	0·000	n.c.	n.c.	n.c.	n.c.
H_2O	2·000	n.c.	2·000	n.c.	n.c.	2·000	n.c.	n.c.	n.c.	n.c.
Total	7·746	5·105	7·735	2·000	2·999	7·725	5·008	3·999	3·997	4·001

n.c., not calculated; n.d., not determined. Mineral abbreviations according to Kretz (1983). Formula calculations: Bt, 11 oxygens, 2 OH, all Fe as Fe^{2+}; Kfs, Plg, 8 oxygens, all Fe as Fe^{3+}; Spl, 4 oxygens, 3 cations, Fe^{3+} from charge balance; Ilm, 3 oxygens; Opx, Cpx, 6 oxygens.

Feldspars

In migmatites, plagioclase displays An contents between 14 and 41 mol %, the most An-rich plagioclase grains occurring as inclusions in garnet. Plagioclase may show K_2O contents up to 0·7 wt %. There is no systematic compositional difference between plagioclase grains in leucosomes and those in mesosomes. Single plagioclase grains may show weak compositional zoning or domains, but very unsystematically. K-feldspars in migmatites are mostly perthitic on different scales. The lamellae are almost pure albite, situated in orthoclase with ~2 wt % Na_2O. Plagioclase in mafic granulites is less enriched in albite component than in migmatites, and in magnetite-bearing rocks plagioclase is very rich in anorthite (up to 99 mol %).

Other phases

Ilmenites have uniform compositions with X_{Mg} values ranging between 0·01 and 0·05, and TiO_2 contents of 51·1–52·8 wt %. Single ilmenite grains are homogeneous. Spinels in all samples are also compositionally fairly uniform with X_{Mg} values of 0·020–0·204. Spinels are characterized by different ZnO contents in different

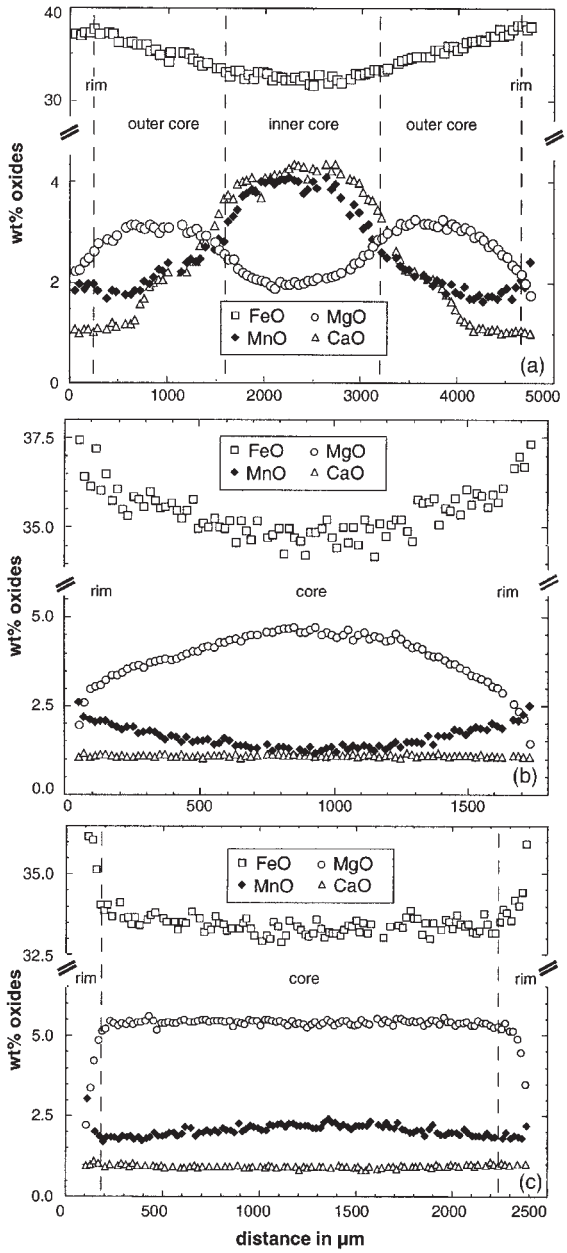

Fig. 6. Garnet zoning patterns. (a) Garnet, type gI. (b) Garnet, type gII. (c) Garnet, type gIII. (For further explanation, see sections on petrography and on mineral chemistry.)

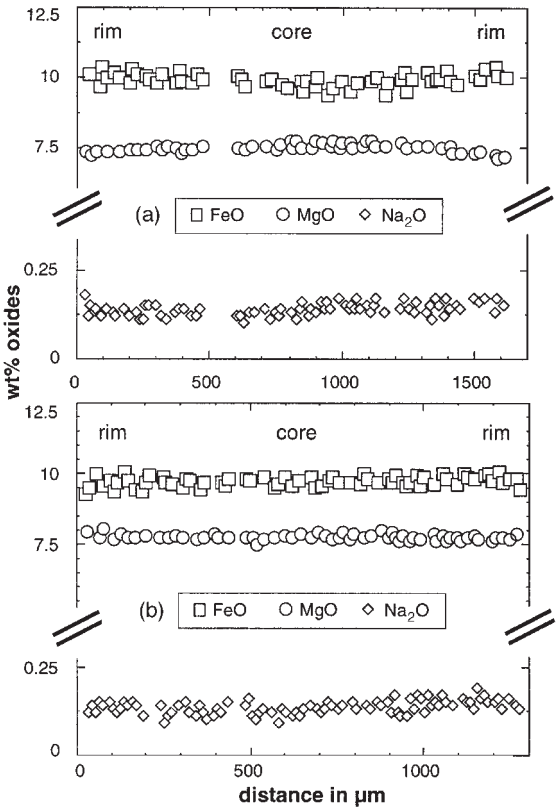

Fig. 7. Cordierite zoning patterns. (a) Sample BW-45; a very small rimward decrease of X_{Mg} can be observed. (b) Sample BW-13c; completely flat zoning pattern. (For further explanation, see sections on petrography and on mineral chemistry.)

samples (0·8–4·8 wt %). Single spinel grains are homogeneous regarding all element contents. Sillimanites may have small amounts of Fe_2O_3 (0·0–0·4 wt %).

METAMORPHIC EVOLUTION

Fluids

For migmatites of the Bayerische Wald, the occurrence of magnetite is restricted to the Silberberg ore (see section on petrography), which has probably experienced specific fluid environments and O_2 fugacities that do not apply to the majority of the migmatites. In the latter, the ubiquitous presence of graphite with pyrrhotite and/or pyrite instead of magnetite during stages A–D points to comparatively low O_2 and high S_2 fugacities (Shi, 1992). Additionally, the assemblage limits X_{H_2O} in any possibly coexisting fluid to 0·05–0·1 at conditions of 800–850°C and 0·5 GPa (Poulson & Ohmoto, 1989; Connolly & Cesare, 1993). The occurrence of primary N_2 and secondary CO_2 in quartz inclusions in garnets (type gI inner or outer cores) suggests an N_2–CO_2 fluid phase during late stage A and at the beginning of stage B. Cordierites coexisting with gI outer cores and gII garnets at stage B (cII–cIV) have accommodated N_2, CO_2 and H_2O in their channels. The H_2O and CO_2 channel contents are far below the experimentally determined values for fluid-saturated conditions (Johannes & Schreyer, 1981) and indicate that the cordierites from the Bayerische Wald cannot have equilibrated with an H_2O- or CO_2-dominated fluid phase at stage B. The observed H_2O channel contents are similar to those of cordierites experimentally

equilibrated with a peraluminous water-undersaturated melt (Carrington & Harley, 1996) and are consistent with dehydration melting in the absence of an aquous fluid during stage B in migmatites of the Bayerische Wald. The low CO_2 contents of cordierites and the CO_2 and N_2 fluid inclusions in quartz hosted by garnet may suggest the presence of a nitrogen-dominated N_2–CO_2 fluid during late stage A and early stage B. As CO_2 and N_2 are known to lower dry solidus temperatures only insignificantly (Keppler, 1989: haplogranitic system; Clemens *et al.*, 1997: system $KAlO_2$–SiO_2–MgO) the onset of melting in fluid-absent dehydration melting experiments can be used as a minimum temperature estimate for migmatites of the Bayerische Wald.

Mineral reactions

Textures imply that mineral assemblages of stages A–D are related by a number of reactions. As the bulk compositions of the migmatites from the Bayerische Wald are roughly represented by the system K_2O–FeO–MgO–Al_2O_3–SiO_2–H_2O (KFMASH), qualitative grids for KFMASH (e.g. Fitzsimons, 1996; Greenfield *et al.*, 1998; Raith & Harley, 1998; Whittington *et al.*, 1998) can in principle be used to illustrate stable univariant reactions and their relative positions in P–T space. The published grids and pseudosections mainly consider variations in the SiO_2/(FeO + MgO) ratio (Fitzsimons, 1996), in X_{Mg} (Raith & Harley, 1998) or in X_{Al} {X_{Al} = (Al – K)/[(Al – K) + Fe + Mg], Greenfield *et al.*, 1998}. The results of dehydration melting experiments performed with similar compositions can also be used to constrain possible reactions. The starting compositions mainly account for variations in X_{Mg}, and in SiO_2 and Al_2O_3 contents and ratios. They allow for some minor additional components such as TiO_2, CaO and Na_2O that are present in natural migmatites and for the at least divariant character of most reactions. Thus, dehydration melting experiments and KFMASH grids are used to constrain a qualitative P–T path for migmatites of the Bayerische Wald.

The determination of correct bulk compositions necessary for this approach is problematic for migmatites of the Bayerische Wald. One reason is that the mesosomes and melanosomes hosting the reaction relics to be used as P–T monitors have experienced varying degrees of melt extraction and different scales of melt segregation, implying that size and composition of the bulk systems before melting are not really known. This applies particularly to bulk Al_2O_3 and SiO_2 contents and ratios as reflected by the decrease of modal quartz and the increase of modal sillimanite with increasing degree of melt extraction in the order undifferentiated migmatite (MIG1)–weakly depleted mesosome (MIG3)–depleted mesosome (MIG2)–melanosome (MIG4). In contrast, X_{Mg} is not very sensitive to melt removal as the only minor amounts of Fe–Mg phases crystallizing from melt in leucosomes cannot change X_{Mg} in the restitic parts significantly. Therefore, X_{Mg} values in MIG1 migmatites, in MIG2–MIG4 mesosomes and melanosomes, and in orthopyroxene-bearing migmatites approximate bulk X_{Mg} values. They show only limited variations (0·42–0·60).

Another difficulty in determining correct bulk compositions is the small-scale mineralogical heterogeneity, reflected by the large range in modal composition for each migmatite type. Although the relation between modal quartz and sillimanite and the degree of melt extraction is generally as aforementioned, many domains within melanosomes and mesosomes of MIG2 and MIG4 types may be entirely quartz or sillimanite absent whereas others are fairly quartz or sillimanite rich. Similarly, although average X_{Mg} values show only little variation, many migmatite domains differ significantly in their X_{Mg} values, as is evident from drastically differing modal abundances and ratios of garnet (X_{Mg} 0·01–0·31), biotite (X_{Mg} 0·24–0·53) and cordierite (X_{Mg} 0·41–0·74). Hence, chemical domains in the millimetre to centimetre range rather than larger-scale bulk compositions control mineral reactions, but their compositions cannot be precisely determined.

Stage A reactions

The reactions forming gI inner cores cannot be constrained, because of the lack of suitable inclusions. The zoning patterns preserved in gI inner cores (Fig. 6a) are hardly affected by later diffusion, because of the large grain size. They correspond to the growth patterns commonly found in low- to medium-grade metapelites (Chakraborty & Ganguly, 1990), which may also be derived by modelling (Loomis, 1986). Therefore, temperature probably increased during growth of gI garnet cores. The lack of sillimanite inclusions in the inner cores and their presence in the outer cores of type gI garnets might indicate garnet formation at stage A outside the sillimanite stability field. The comparatively high CaO contents in the inner cores of gI garnets may point to garnet formation at higher pressures than for the outer cores. However, the abrupt decrease in CaO contents may also be due to a simple change in the garnet-forming reaction, caused by the exhaustion of a reactant Ca-bearing phase.

Between stages A and B sillimanite was formed in MIG1–MIG4 migmatites and in magnetite-bearing rocks. The reaction cannot be constrained as the small sillimanite needles contain no inclusions. The rare aggregates of sillimanite within cordierite that seem to pseudomorph larger blades or laths may perhaps point to early stage A kyanite (Fig. 5i).

Stage B reactions

Various lines of evidence (see section on evidence for partial melting) indicate dehydration melting during stage B. KFMASH topology (e.g. Fitzsimons, 1996) predicts that the first dehydration melting reactions to occur with rising temperatures in quartz-bearing pelitic compositions are the divariant reactions

$$\text{bt} + \text{sil} + \text{qtz} = \text{grt} + \text{Kfs} + \text{L} \quad (1)$$

and

$$\text{bt} + \text{sil} + \text{qtz} = \text{crd} + \text{Kfs} + \text{L}. \quad (2)$$

This accounts for leucosome formation and for the inclusion assemblages in gII garnets, gI outer cores (Figs. 5d, h) and cII cordierites (Fig. 5b). The reactions probably also formed cI cordierites (Fig. 5a) and gIII garnets that are compositionally similar to gII garnets. CI cordierites and gIII lack significant inclusions, but are associated with K-feldspar, quartz and minor biotite in leucosomes.

Dehydration melting experiments have confirmed that at crustal pressures of 0·5–1·0 GPa (Le Breton & Thompson, 1988; Vielzeuf & Holloway, 1988; Patiño Douce & Johnston, 1991; Vielzeuf & Montel, 1994; Carrington & Harley, 1995; Gardien *et al.*, 1995; Patiño Douce & Beard, 1996; Stevens *et al.*, 1997; Montel & Vielzeuf, 1997) quartz-bearing pelites with high X_{Mg} produce cordierite at near-solidus conditions, those with low X_{Mg} garnet and those with intermediate X_{Mg} both (Fig. 8). This explains why in the migmatites of the Bayerische Wald, where X_{Mg} can vary on the millimetre to centimetre scale, cordierite (cI, cII) and garnet (gII, gIII, gI outer cores) may either form in different sites or be intergrown. Dehydration melting experiments with starting compositions varying in Al_2O_3 contents (quartz-bearing pelites and greywackes; e.g. Stevens *et al.*, 1997) show that at the pressures of interest, orthopyroxene is formed at near-solidus conditions via the reaction

$$\text{bt} + \text{qtz} + \text{plg} = \text{crd} + \text{grt} + \text{opx} + \text{L} \pm \text{Kfs} \quad (3)$$

if Al_2O_3 contents are very low and/or if X_{Mg} is fairly high (Fig. 8). This accounts for the simultaneous formation of orthopyroxene, garnet and cordierite in the orthopyroxene-bearing migmatites of the Bayerische Wald (Fig. 5j), where the lack of sillimanite indicates low bulk Al_2O_3 contents.

For quartz-free pelites, KFMASH topology (e.g. Fitzsimons, 1996) predicts formation of spinel during dehydration melting via the reaction

$$\text{grt} + \text{bt} + \text{sil} = \text{crd} + \text{spl} + \text{Kfs} + \text{L} \quad (4)$$

and subsequent consumption of spinel via the reaction

$$\text{spl} + \text{bt} + \text{sil} = \text{crd} + \text{Kfs} + \text{L}. \quad (5)$$

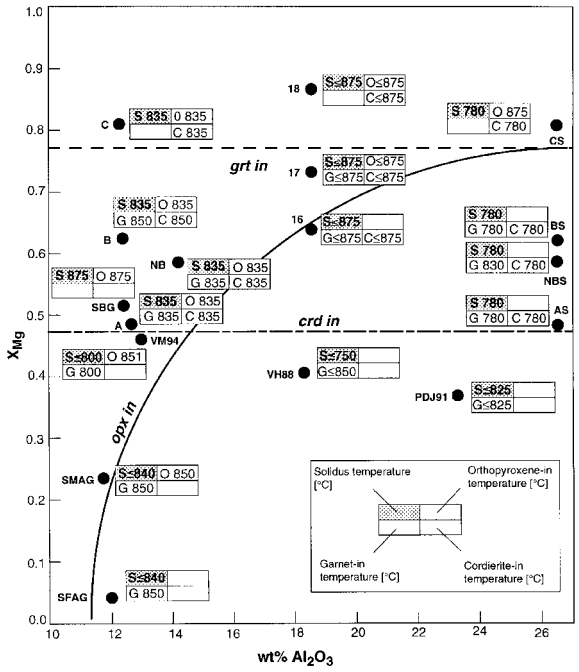

Fig. 8. Compilation of solidus temperatures and solid phases produced during dehydration melting experiments at 0·5–0·7 GPa in a plot of bulk Al_2O_3 vs bulk X_{Mg}. PDJ91, Patiño Douce & Johnston (1991); VH88, Vielzeuf & Holloway (1988); VM94, Vielzeuf & Montel (1994); SBG, starting composition of Patiño Douce & Beard (1995); SFAG, SMAG, starting compositions of Patiño Douce & Beard (1996); A, B, C, NB, AS, BS, CS, NBS, starting compositions of Stevens *et al.* (1997); 16, 17, 18, starting compositions of Carrington & Harley (1995). Shown are results of experiments at 0·5 GPa except where not available (PDJ91, 0·7 GPa; VH88, 0·7 GPa; 16, 17, 18, 0·5–0·7 GPa). '≤' indicates that no runs were performed at lower temperatures with the respective compositions. The lines labelled 'opx in', 'grt in' and 'crd in' were graphically fitted to the data shown in the diagram.

In migmatites of the Bayerische Wald, reaction (4) probably accounts for intergrowths of garnet (gI, gII), K-feldspar, cordierite (cIV), sillimanite, spinel and biotite (Fig. 5h) and for the cores of cIII cordierites that contain spinel with sillimanite inclusions. Reaction (5) probably produced the inclusion-free rims of cII and cIII cordierites. An alternative explanation for these rims is that cII and cIII cordierites reacted with melt (spl + L = crd; Blümel & Schreyer, 1976; Komatsu *et al.*, 1994). The presence of quartz inclusions in most garnets supports the contention that quartz deficiency is not a primary feature but was caused by extraction of a silica-rich melt during stage B (see above). At near-solidus conditions spinel has been detected as a very minor product phase in only a few dehydration melting experiments with compositions low in X_{Mg} at 0·5–0·7 GPa. This is probably due to the fairly quartz-rich starting materials where spinel is stable only at sites of local silica deficiency.

K-feldspar is treated as a product in KFMASH grids and is present as a product in many dehydration ex-

periments. However, Carrington & Watt (1995) have argued that K-feldspar may be a reactant in dehydration melting if biotite has a higher H_2O/K_2O than melt. In migmatites of the Bayerische Wald, microstructures of K-feldspar and quartz-dominated leucosomes (Berger & Kalt, 1999), biotite and quartz inclusions in leucosome feldspars as well as garnet–K-feldspar and cordierite–K-feldspar intergrowths in mesosomes and melanosomes are consistent with K-feldspar being a product of dehydration melting. However, rare inclusions of K-feldspar in garnet and the lack of K-feldspar in some mesosomes and melanosomes may also be interpreted as the contrary case.

Textures in migmatites of the Bayerische Wald indicate that reactions (1)–(5) have not gone to completion. In all cases, biotite is left over and is present either as inclusion or as neighbouring phase to the solid products of partial melting (cordierite, garnet, orthopyroxene, spinel). In quartz-rich and sillimanite-absent domains (preferably in MIG1 and MIG3 migmatites) the lack of sillimanite probably arrested the reactions, whereas in spinel-rich domains the lack of quartz probably caused the termination. However, gII garnets, orthopyroxenes and cIII cordierites contain all reactants to reactions (1), (3) and (5), respectively, suggesting that the latter were terminated for reasons other than consumption of one of the reactants and that biotite was stable. However, it is difficult to distinguish between restitic biotite and biotite crystallized from melt as there are no clear textural or compositional differences (see sections on mineral chemistry and quantitative *P–T* path).

In the almost biotite-free magnetite-bearing rocks, textures suggest that no melt was produced at stage B. Intergrowths of garnet, spinel, quartz and cordierite with sillimanite inclusions in garnet and spinel may be best explained by the KFMASH reaction

$$\text{grt} + \text{sil} = \text{spl} + \text{qtz} + \text{crd}. \quad (6)$$

Mineral reactions leading to stage B parageneses in mafic granulites cannot be constrained, because of the lack of suitable inclusions.

Stage C reactions

Stage C is characterized by crystallization of the melt formed at stage B. In massive MIG1 migmatites, melt was not extracted but crystallized at the site of production as indicated by the lack of distinct leucosomes and the existence of only vaguely distinguishable light areas. Crystallizing phases are plagioclase, quartz, K-feldspar and probably also biotite. The embayed and skeletal biotite shapes that are intimately intergrown with fine-grained quartz and feldspars (Fig. 5c) may represent former sites of melt crystallization. The fact that these microtextures are either restricted to the outer parts of grains or associated with common blocky biotite suggests that melt probably crystallized in places where restitic biotite was left over from dehydration melting. In MIG3 migmatites, only some of the melt was segregated to crystallize in leucosome sites. This contention is supported by the only minor quartz and feldspar depletion in mesosomes, by their diffuse margins with leucosomes and by the same melt crystallization features in mesosomes as described for MIG1 migmatites (Fig. 5c, see above). The last two observations hold true also for orthopyroxene-bearing migmatites.

In MIG2 and MIG4 migmatites, most of the melt segregated into leucosomes, consistent with the strong quartz and feldspar depletion in mesosomes and melanosomes, and with their sharp margins with leucosomes. Two assemblages are stable at stage C in leucosomes: Plg + Kfs + qtz ± crd ± grt ± bt and Kfs + qtz. The former show microstructural evidence for rheological behaviour of a crystal mush (Berger & Kalt, 1999) and were hence not pure melts but contained solid 'restitic' phases, specifically plagioclase, garnet and cordierite. The latter show microstructural and compositional evidence for having been virtually pure melts (Berger & Kalt, 1999). Rare intergrowths of fabric-forming biotite with sillimanite and quartz adjacent to garnet (Fig. 5e) and K-feldspar in MIG3 and MIG4 migmatites probably reflect melt crystallization in mesosomes and melanosomes via the KFMASH reaction grt + Kfs + L = bt + sil + qtz (1).

Although the channel volatile contents of cordierite indicate that the melt formed at stage B was H_2O undersaturated, it is possible that melts reached H_2O saturation during progressive crystallization at stage C. However, there is no indication for release of significant amounts of a hydrous fluid at stage C. The hydration reactions observed in migmatites of the Bayerische Wald such as pinitization of cordierite, sericite formation in plagioclase, and muscovite and chlorite formation from biotite occur at temperatures far below the lower thermal stability of H_2O-saturated melts. Only the fine-grained melt crystallization textures of biotite (Fig. 5c) could perhaps be interpreted as fluid-present textures reflecting relatively high temperatures, similar to myrmekites in granites. In summary, it can be concluded that formation of cordierite during the melting process and formation of biotite during melt crystallization largely kept pace with H_2O saturation of the melts.

Stage D reactions

In a few MIG3 and MIG4 samples, postkinematic cordierite (cV) formed around garnet wherever garnet was bordered by biotite intergrown with sillimanite and quartz (Fig. 5e). The reaction

$$\text{grt} + \text{sil} + \text{qtz} = \text{crd} \quad (7)$$

probably accounts for this texture. The fact that cV cordierites grew at the expense of biotite–sillimanite–quartz intergrowths that probably reflect melt crystallization (see above) suggests that melt had crystallized before stage D. In magnetite-bearing rocks, the cordierite–spinel–magnetite textures (Fig. 5k) indicate that a former complex spinel exsolved spinel and magnetite (and ilmenite) after the growth of cordierite seams, as the latter have approximately the same width between magnetite and quartz as they have between spinel and quartz. At stage D, the spl_{ss}–qtz contacts obviously became unstable and cordierite rims grew according to the reaction

$$spl_{ss} + \text{qtz} = \text{crd}. \quad (8)$$

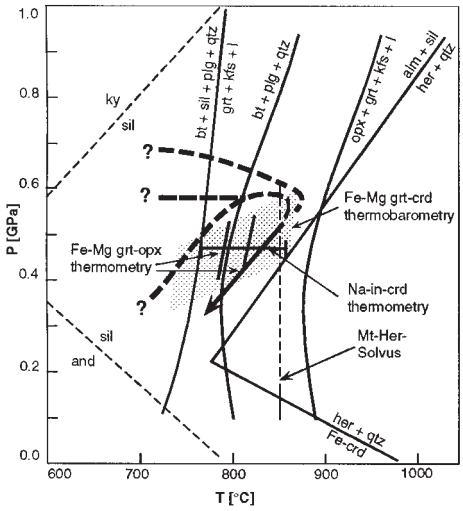

Fig. 9. *P–T* diagram showing qualitative and quantitative temperature and pressure constraints as well as possible *P–T* paths for migmatites of the Bayerische Wald. The metapelite solidus (bt + sil + plg + qtz = grt + Kfs + L) is taken from Le Breton & Thompson (1988) and represents a minimum temperature for MIG1–MIG4 migmatites. The divariant metagreywacke dehydration melting reaction (bt + plg + qtz = opx + grt + Kfs + L) is taken from Vielzeuf & Montel (1994), whereby the solidus is a minimum and the biotite-out curve a maximum temperature estimate for orthopyroxene-bearing migmatites. The magnetite–hercynite solvus (Fe_2O_3–FeO–Al_2O_3 system) is from Turnock & Eugster (1962) and approximates minimum temperatures for the magnetite-bearing samples. It should be noted that Zn, Mg and Ti in spinel may shift the solvus. The reaction alm (almandine) + sil = her (hercynite) + qtz (FAS system; Bohlen *et al.*, 1986) was crossed by the magnetite-bearing rocks towards the high-temperature side on the prograde path. The reaction her + qtz = crd (FAS system; Bohlen *et al.*, 1986) was crossed towards the low-pressure side on the retrograde path by the magnetite-bearing rocks. It should be noted that Mg in cordierite and Fe^{3+}, Zn and Ti in spinel will shift the position of the two reactions involving hercynite. The fields and lines indicate the results of geothermobarometry (see Table 6 for further information) and include 2σ errors. (For further information, see section on quantitative *P–T* constraints.)

Qualitative *P–T* path

Prograde zoning patterns of gI garnet inner cores indicate rising temperatures during stage A. Equivocal pseudomorphs after kyanite could indicate this temperature rise to be within the kyanite stability field. During stage B, the migmatites crossed different biotite dehydration melting curves [reactions (1)–(5)] in the absence of an aqueous fluid phase. The experimentally determined solidus curves for various bulk systems (Fig. 9 and section on mineral reactions) have very steep, mainly positive slopes in *P–T* space. Magnetite-bearing rocks crossed reaction (6), which also has a fairly steep positive slope in the FAS system (Bohlen *et al.*, 1986, Fig. 9). Hence, MIG1–MIG4 migmatites and their intercalations experienced a further temperature increase during stage B. Sillimanite inclusions in garnet, spinel and cordierite indicate this temperature rise including melting to be within the stability field of sillimanite.

During stage C, the steep biotite dehydration reactions (1)–(5) were crossed from the high- to the low-temperature side as melt crystallized, indicating decreasing temperatures. The rocks cooled within the stability field of sillimanite as suggested by sillimanite–biotite–quartz intergrowths that are interpreted as crystallization features. Hence, stage B includes a prograde stage, peak conditions and the retrograde path down to melt crystallization, which is still at very high temperatures (see section on quantitative *P–T* constraints). The metamorphic path between stages B and C is characterized by further cooling within the stability field of cordierite and sillimanite.

Stage D is characterized by two subsolidus cordierite-forming reactions [(7) and (8)] that have very flat slopes in *P–T* space with cordierite always on the low-pressure side. Reaction (7) (FAS system; Mukhopadhyay & Holdaway, 1994) has a positive slope whereas reaction (8) (FAS system; Bohlen *et al.*, 1986) has a negative slope. It is therefore most likely that stage D is mainly characterized by decompression.

In conclusion, the *P–T* path for migmatites and gneisses of the Bayerische Wald is either clockwise (if the kyanite stability field was passed during stage A, Fig. 9) or characterized by largely identical prograde and retrograde parts of the loop (if the kyanite stability field was not passed during stage A, Fig. 9).

QUANTITATIVE *P–T* CONSTRAINTS

Constraints from experiments

For stage B, the presence of sillimanite at melting temperatures limits pressures to below 1·0 GPa approximately

Table 6: Calculated temperatures and pressures

Sample	Na in Crd (c.p.f.u.)	$T_{Na(M86)}$ (°C)	$T_{gc(B88)}$ c (°C)	$T_{gc(B88)}$ r (°C)	T, $P_{gc(MS81)}$ c (°C, GPa)	$T_{go(H94)}$ (°C)	$T_{2px(W77)}$ (°C)
BW-06	0·035±0·006	784±15					
BW-13a	0·021±0·004	819±10	830±27	712	860, 0·51		
BW-13c	0·026±0·004	807±10	846±33	727	860, 0·51		
BW-18	0·026±0·005	807±13	796±29	690	810, 0·48		
BW-19	0·023±0·007	814±18	827±32	637	825, 0·50		
BW-28	0·034±0·005	787±13	688±35	634	720, 0·38		
BW-29	0·023±0·005	814±13	784±37	628	880, 0·46		
BW-34	0·029±0·004	799±10	778±29	692	828, 0·44		
BW-36	0·016±0·005	832±13	811±35	684	800, 0·48		
BW-44M	0·026±0·005	807±13	790±36	626	825, 0·47		
BW-45	0·026±0·005	807±13	807±28	582	850, 0·46		
BW-46	0·023±0·006	814±15	816±37	596	850, 0·46		
BW-66	0·024±0·005	812±13	818±32	760	848, 0·50		
BW-81	0·025±0·004	809±10	841±39	711	845, 0·50		
BW-83	0·013±0·004	837±10	795±34	675	840, 0·46		
BM-01L	0·020±0·004	822±10					
BM-01M	0·021±0·008	819±21	797±35	585	885, 0·48		
E-22L	0·038±0·006	777±15					
E-22M	0·035±0·005	784±13	637±34	568	740, 0·33		
BW-20*	0·011±0·005		770±39	679	848, 0·45		
86246*	0·009±0·005		838±32	639	848, 0·51		
BL-1	0·031±0·004	793±10	787±39	708	780, 0·49	799±31	
BW-39							879±22

Mineral abbreviations according to Kretz (1983); c, outer core composition of garnet, core composition of cordierite (Fig. 4, section on mineral chemistry); r, rim compositions of garnet and cordierite; $T_{Na(M86)}$, temperature calculated using the Na-in-cordierite thermometer of Mirwald (1986); $T_{gc(B88)}$, temperature calculated using the garnet–cordierite thermometer of Bhattacharya *et al.* (1988); $T,P_{gc(MS81)}$, temperature and pressure derived graphically from intersection of Mg isopleths for cordierite and garnet in P–T space at $X_{H_2O} = 0$ on the basis of the calculation by Martignole & Sisi (1981). $T_{go(H94)}$, temperature calculated using the garnet–orthopyroxene thermometer of Harley (1984); $T_{2px(W77)}$, temperature calculated using the two-pyroxene thermometer of Wells (1977). Errors are 2σ errors. No errors can be given on rim temperatures because of the strong zoning of garnet rims (see Fig. 4 and section on mineral chemistry) and for graphically derived best fits.
*Only calcic plagioclase is present in these samples, meaning that the requirement for use of the Na-in-cordierite thermometer is not met (see Introduction).

(Fig. 9). The lack of cordierite at the solidus over a wide range of Al_2O_3 bulk contents in several dehydration melting experiments at 1·0 GPa (e.g. Le Breton & Thompson, 1988; Vielzeuf & Holloway, 1988; Gardien *et al.*, 1995) and its presence in many 0·5–0·7 GPa experiments with suitable compositions (Stevens *et al.*, 1997) along with its ubiquitous occurrence in the migmatites of the Bayerische Wald argue for melting in the latter at low pressures. Hence, 0·5 and 0·7 GPa experiments should be used to determine minimum temperatures for stage B. At these pressures, aluminous compositions (pelites) of variable X_{Mg} start to melt at $\leq$780°C with cordierite and garnet produced as solid phases (Stevens *et al.*, 1997). Less aluminous compositions (greywackes) of variable X_{Mg} start to melt at $\leq$800°C (Vielzeuf & Montel, 1994) to $\leq$835°C (Stevens *et al.*, 1997) with cordierite, garnet and orthopyroxene formed. The latter temperatures are minimum estimates for the orthopyroxene-bearing migmatites of the Bayerische Wald and hence for the entire tectonometamorphic unit.

Minimum temperatures for stage B may be deduced from the fact that in magnetite-bearing rocks the intergrowths of magnetite, spinel and ilmenite (Fig. 5k) indicate formation of a primary solid solution above the spinel–magnetite solvus (Turnock & Eugster, 1962). The compositions of now coexisting spinel and magnetite have been subject to retrograde re-equilibration, as is evident from very low Al_2O_3 contents in magnetite and very low Fe_2O_3 contents in spinel. The reintegrated volume percentages of spinel and magnetite components suggest

a former intermediate composition but are fraught with large errors. Moreover, the effects of ZnO, MgO and TiO_2 (all present in minor amounts; see Table 5) have not been considered in the $FeO–Fe_2O_3–Al_2O_3$ experiments of Turnock & Eugster (1962). Hence, their maximum solvus temperature of ~850°C at intermediate compositions cannot readily be taken as a minimum estimate for migmatites of the Bayerische Wald. Moreover, thermobarometry on the cordierites formed between the complex spinel and quartz before exsolution indicate lower temperatures (see section on thermobarometry and Table 6).

As biotite was stable through stages A–D in migmatites of the Bayerische Wald (see section on mineral reactions), maximum temperatures for stage B can be obtained from comparison with biotite-out temperatures in the relevant dehydration melting experiments. As most partial melting reactions are at least divariant, biotite is stable with melt through a temperature interval. If neither sillimanite nor quartz deficiency terminates the dehydration melting reactions, biotite-out temperatures mainly depend on TiO_2 and F contents of biotites (e.g. Stevens *et al.*, 1997), with F contents often not being available. TiO_2 incorporation obviously stabilizes biotite to higher temperatures. At 0·5–0·7 GPa, the lowest biotite-out temperatures are 875°C with initial TiO_2 contents of 1·0–1·78 wt % (Vielzeuf & Holloway, 1988; Patiño Douce & Beard, 1996) and the highest temperatures are 950°C with initial TiO_2 contents of 3·9 wt % (Patiño Douce & Beard, 1995). In these experiments, biotite is enriched in TiO_2 in the course of dehydration melting. In migmatites of the Bayerische Wald, biotites show large intrasample variations in TiO_2, consistent with the fact that single grains were involved in partial melting and retrograde re-equilibration to different degrees. The lowest TiO_2 contents of biotites (2·3 wt %) may approximate the initial compositions and suggest a very crude upper temperature limit for stage B of ~900°C.

A similar maximum temperature is indicated by the lack of spinel–quartz assemblages in the migmatites of the Bayerische Wald. In the FMASH system (Hensen & Green, 1973) and in most dehydration melting experiments at 0·5–0·7 GPa (e.g. Stevens *et al.*, 1997), spinel–quartz assemblages become stable above ~900–950°C as a result of the breakdown of garnet–sillimanite assemblages. In the Bayerische Wald, coexisting spinel and quartz are found only in the magnetite rocks, where Fe^{3+} stabilizes spinel to lower temperatures (Dasgupta *et al.*, 1995).

As stage C is characterized by crystallization of the melt formed during stage B, the temperatures for the onset of dehydration melting reactions (see above) are maximum temperatures for this stage. During subsequent stage D, spinel + quartz in magnetite-bearing rocks broke down to form cordierite. In the FAS system, this reaction occurs at maximum conditions of 0·2 GPa and 780°C (Bohlen *et al.*, 1986), where it is terminated by other reactions. However, the significant MgO contents of cordierite in the magnetite-bearing rocks probably shift this reaction to higher pressures.

Geothermobarometry

For metapelitic rocks, a number of geothermometers and geobarometers can be used to quantify *P–T* conditions. Phase equilibria involving Ca exchange between garnet and other phases (e.g. Koziol & Newton, 1988) are not applicable to the migmatites investigated here, as the Ca contents of garnets are very low and Ca contents of garnets are known to not necessarily reflect equilibrium (Chernoff & Carlson, 1997). Phase equilibria involving garnet, rutile and ilmenite (e.g. Bohlen *et al.*, 1983; Bohlen & Liotta, 1986) are also not applicable because of the lack of significant amounts of rutile in the migmatites of the Bayerische Wald. Here, garnet–cordierite, garnet–orthopyroxene, Na-in-cordierite and two-pyroxene temperatures were calculated.

In migmatites of the Bayerische Wald, all phases except for garnets have largely uniform compositions except for their outermost rims (see section on mineral chemistry). It must be concluded that they continuously equilibrated on the retrograde path down to stage D. Only garnets have not been completely re-equilibrated, because of their large grainsize and their low diffusion velocities for most elements compared with other phases. Hence, for geothermometry on migmatites of the Bayerische Wald, it is to be expected that peak temperatures (stage B) cannot be retrieved. For all geothermobarometric calculations, the outermost rims of minerals were not considered, because of comparatively steep zoning patterns (Figs 6 and 7) that reflect non-equilibrium.

Pressure-independent temperature estimates can be made for cordierite-bearing metamorphic rocks that contain fairly sodic plagioclase ($An \leq 40$ mol %) by using the Na contents of cordierite (Mirwald, 1986; Kalt *et al.*, 1998). For all cordierite-bearing samples, except samples BW-20 and 86246, which contain very calcic plagioclase, Na-in-cordierite temperatures were calculated and values between 777 and 837°C were obtained (Table 6) using the mean Na contents of cordierite in each sample (Fig. 10). As expected, there is no significant and systematic temperature difference between the different cordierite types (cI–cV).

Pressure-dependent garnet–cordierite Fe–Mg exchange temperatures can be calculated for all garnet- and cordierite-bearing samples. According to textural observations (see section on petrography), cII–cIV cordierites coexist with gI garnet outer cores and with gII garnet cores at stage B. The gI outer cores and gII cores have been affected by retrograde exchange, probably

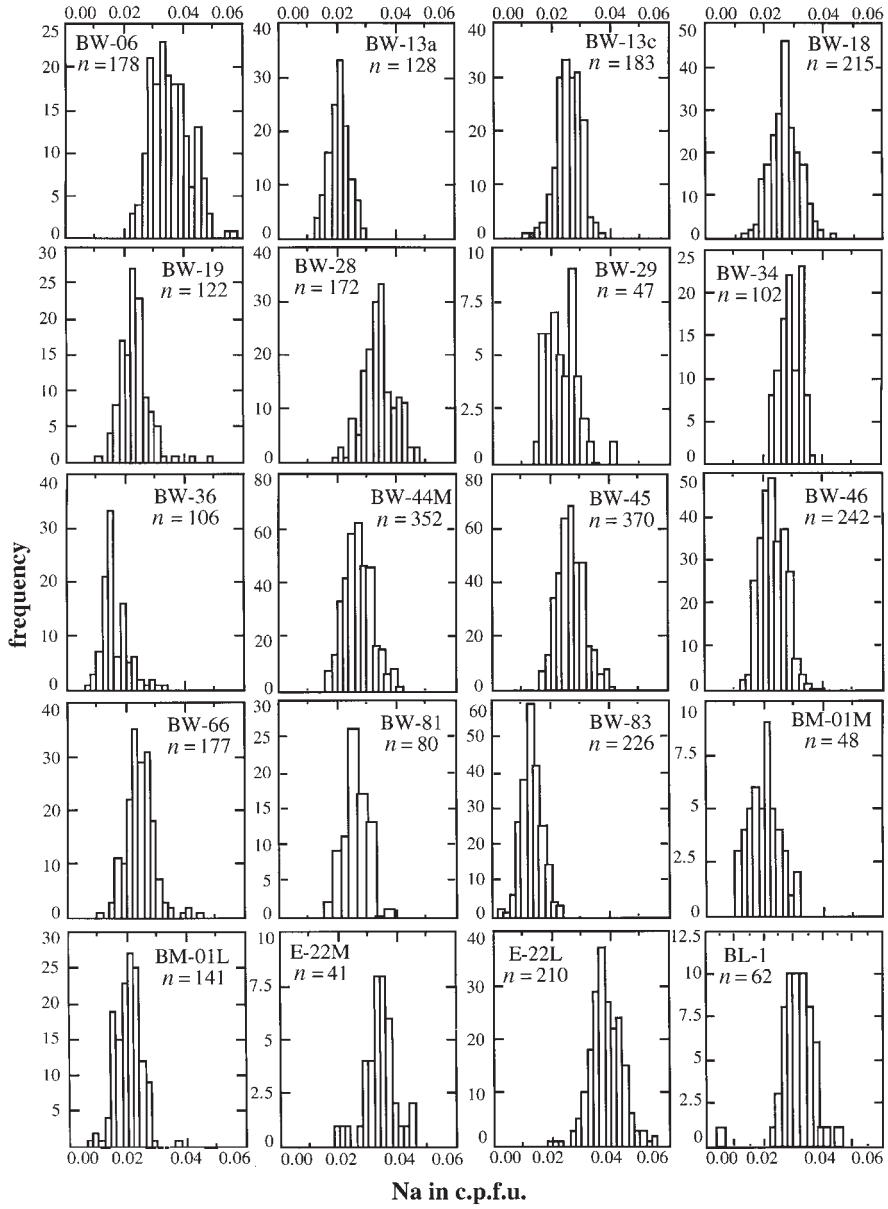

Fig. 10. Na contents of cordierites from the studied samples. The data are presented as histograms (frequency plotted against Na contents in c.p.f.u.). *n* represents the number of analyses. Mean values, precision, and temperatures calculated with the Na-in-cordierite thermometer of Mirwald (1986) are given in Table 6.

with biotite, as is evident from rimward-increasing MnO and FeO and rimward-decreasing MgO. Compositions in the centre of gI outer cores and gII cores have the highest X_{Mg} values and are compositionally similar to largely unzoned gIII garnets that formed at the same time, but do not coexist directly with cordierite. These values are probably the best approximation to the original composition and were thus taken for garnet–cordierite thermometry. However, as stated above, these temperatures will reflect retrogression and not peak conditions. Using the respective compositions and applying the garnet–cordierite thermometer formulation of Bhattacharya *et al.* (1988) assuming a pressure of 0·5 GPa yields temperatures between 770 and 846°C (Table 6), which coincide with those calculated by Na-in-cordierite thermometry. The same temperature range is obtained

when applying the thermometer to gI garnet outer cores and gII garnet cores in contact with cV cordierites (stage D). Garnet–cordierite core temperatures for orthopyroxene-bearing migmatites are 787°C and those for magnetite-bearing rocks 770 and 838°C (Table 6).

Mg–Fe partitioning between garnet and cordierite is a function not only of temperature, but also of pressure and water activity (Martignole & Sisi, 1981; Mukhopadhyay & Holdaway, 1994). Choosing the appropriate isopleths of Martignole & Sisi (1981) for cII–cIV cordierites and coexisting gI garnet outer cores and gII garnet cores (stage B) at low water activities (0·0–0·1) as appropriate for the investigated case (see section on fluids) gives approximate equilibrium conditions of 780–885°C and 0·44–0·51 GPa (Fig. 9).

Two samples give distinctly lower temperatures of 688°C (BW-28) and 637°C (E-22M) when the grt–crd thermometer of Bhattacharya *et al.* (1988) is applied. The Mg–Fe isopleths of garnet and cordierite also yield P–T values in this range (Table 6). Possibly, the very high MnO contents of the garnets in both samples (4–6 wt %) hamper the calculation of realistic Fe–Mg exchange temperatures. However, samples E-22 and BW-28 also record Na-in-cordierite temperatures at the lower limit (777 and 787°C, Table 6) of the entire range. Moreover, these samples contain secondary muscovite. The lower temperatures could thus also be due to local retrograde overprint.

In the orthopyroxene-bearing migmatites, the Fe–Mg exchange between orthopyroxene and garnet can be used to calculate temperatures. Applying the formulation of Harley (1984) to garnet and orthopyroxene core compositions (stage B) and assuming a pressure of 0·5 GPa yields temperatures of 799°C (Table 6). Using the largely pressure-independent pyroxene solvus to determine temperatures in clinopyroxene and orthopyroxene-bearing mafic granulite lenses gives 879°C (stage B) with the formulation of Wells (1977). It must be stressed, however, that the two-pyroxene thermometer is calibrated for peridotite systems.

In summary, the temperatures obtained with diverse thermometers coincide fairly well, although they cover a large range, and are consistent with the minimum and maximum temperature constraints derived from experimental results. However, as phase compositions have obviously re-equilibrated during stage D, the temperatures of 777–846°C obtained by geothermometry are probably below peak conditions and hence only minimum estimates. Pressures of 0·44–0·51 GPa derived from Fe–Mg exchange between garnet and cordierite are also consistent with constraints from experiments and with low water activities.

GEODYNAMIC IMPLICATIONS

Constraints from dehydration melting experiments and thermobarometric calculations used in this study give a minimum estimate of peak metamorphic temperatures during Variscan high-temperature metamorphism in the Bayerische Wald (770–850°C) that are significantly higher than those deduced from similar rocks of the same region in earlier studies on the basis of solid phase equilibria (Schreyer *et al.*, 1964; Blümel & Schreyer, 1976, 1977). The new temperatures are more consistent with the migmatite textures and the very low H_2O contents of cordierites, indicating partial melting in the absence of an aqueous fluid which requires minimum temperatures near 800°C (Le Breton & Thompson, 1988; Gardien *et al.*, 1995).

For the Bayerische Wald, the thermobarometric calculations of this study indicate very high temperatures at shallow crustal levels (0·5 GPa, corresponding to a depth of 15–20 km). Such a temperature–depth distribution in lithosphere or crust previously thickened by collision, as is the case in the Moldanubian zone, is not easily conceivable. The results of models calculating the additional heat input resulting from enhanced radioactive decay caused by crustal thickening (Thompson & Connolly, 1995, and references therein) show that several tens of millions of years would be needed to attain a temperature–depth distribution similar to that deduced for the Bayerische Wald, a time span commonly not available in tectonically active collision zones. Moreover, geochronological data on eclogites and surrounding gneisses in other parts of the Moldanubian zone (Kalt *et al.*, 1994*a*, 1994*b*) suggest the time span between HP metamorphism (collision) and HT–LP metamorphism to be at most 19 Ma considering very conservative error limits. Models considering the thermal effect of rapid tectonic exhumation (e.g. England & Thompson, 1986) predict high temperatures and partial melting in the lower crust, but not at 15–10 km. Hence, an additional heat input is required.

Additional heat input may be achieved by extensive melting in the lithospheric mantle and in the lower crust as a consequence of either downward detachment of thickened lithosphere and its replacement by hot asthenosphere or underplating of mantle-derived magmas (Thompson & Connolly, 1995, and references therein). The Moldanubian zone is characterized by large volumes of mainly S-type granitic rocks. Apart from indicating the entrainment and partial melting of crustal material, the isotopic signatures of these granites suggest the involvement of mantle sources (Gerdes *et al.*, 1995; Langer *et al.*, 1995) and hence point to the existence of mafic melts. The emplacement ages of granitoid magmas in most parts of the Moldanubian zone are only slightly younger than or equal to the age of HT–LP metamorphism (Wendt *et al.*, 1986; Teufel, 1988; Kalt *et al.*, 1994*b*; Siebel, 1995; Schaltegger & Corfu, 1996), indicating that melts were available in the lithospheric mantle and the lower crust at the time of metamorphism.

CONCLUSIONS

(1) On the basis of abundance, geometric relationship, modal composition and microstructures of mesosome, melanosome and leucosome, migmatites in the Bayerische Wald (Bohemian Massif, Variscan Belt, Germany) can be grouped into four types (MIG1–MIG4) and some intercalations that preserve a range of mineral assemblages and reaction textures varying with bulk composition.

(2) All rocks followed the same metamorphic evolution, characterized by a clockwise *P–T* path that can be divided into four stages on the basis of reaction textures and garnet zoning patterns.

(3) Biotite dehydration melting on the prograde path in the absence of an aqueous or carbonic fluid phase produced different solid phases (cordierite, garnet, spinel, orthopyroxene) depending on bulk composition, the latter varying on small and large scale.

(4) Minimum estimates of peak temperatures (800–850°C) and pressure constraints (0·5–0·7 GPa) emerge from experimental results. Mineral equilibria, however, were frozen in on the retrograde part of the *P–T* path at still very high temperatures (770–846°C and 0·44–0·51 GPa) as indicated by homogeneous cordierite compositions and the results of geothermobarometry.

(5) The obtained temperatures are significantly higher than those previously derived for similar rocks of the Bayerische Wald on the basis of subsolidus phase equilibria. The *P–T* path and conditions derived here suggest that high-temperature metamorphism in the Moldanubian zone of the Variscan Belt was induced by anomalously high heat influx to shallow crustal levels of 15–20 km depth subsequent to Variscan collision and crustal thickening.

ACKNOWLEDGEMENTS

The authors would like to thank Udo Geilenkirchen and Ilona Salzmann for preparing numerous polished sections. Michael Eberhardt, Christoph Franzen and Mario Koch are thanked for help with the microprobe work. Thanks also go to Hans-Peter Meyer for maintaining microprobe facilities and for providing formula calculation programs, and to Thomas Ludwig for measuring Li, Be and B contents of some cordierites with the secondary ion mass spectrometer at the Mineralogisches Institut, Heidelberg. Comments by Simon Harley and Rainer Altherr, and reviews by Ian Fitzsimons, Chris Carson and Julie Vry helped to significantly improve the manuscript. Financial support from the Deutsche Forschungsgemeinschaft (Ka 1023/1, Ka 1023/3) within the special research programme 'Orogene Prozesse—ihre Quantifizierung und Simulation am Beispiel der Variziden' is gratefully acknowledged.

REFERENCES

Baburek, J. (1995). High, medium and low pressure assemblages from the Czech part of the Královsky Hvozd Unit (KHU) in the Moldanubian Zone of SW Bohemia. *Journal of the Czech Geological Society* **40,** 115–126.

Beer, W. W. (1981). Die strukturelle Entwicklung der Metamorphite des Bayerischen Waldes. Ph.D. Thesis, University of Göttingen.

Behrmann, J. H. & Tanner, D. C. (1997). Carboniferous tectonics of the Variscan basement collage in the eastern Bavaria and western Bohemia. *Geologische Rundschau* **86,** 15–S27.

Berger, A. & Kalt, A. (1999). Structures and melt fractions as indicators of rheology in cordierite-bearing migmatites of the Bayerische Wald (Variscan Belt, Germany). *Journal of Petrology* (submitted).

Bhattacharya, A., Mazumdar, A. C. & Sen, S. K. (1988). Fe–Mg mixing in cordierite: constraints from natural data and implications for cordierite–garnet geothermometry in granulites. *American Mineralogist* **78,** 681–693.

Blümel, P. & Schreyer, W. (1976). Progressive regional low-pressure metamorphism in Moldanubian metapelites of the northern Bavarian Forest, Germany. *Krystallinikum* **12,** 7–30.

Blümel, P. & Schreyer, W. (1977). Phase relations in pelitic and psammitic gneisses of the sillimanite–potash-feldspar and cordierite–potash feldspar zones in the Moldanubicum of the Lam–Bodenmais area, Bavaria. *Journal of Petrology* **18,** 431–459.

Bohlen, S. (1987). Pressure–temperature–time paths and a tectonic model for the evolution of granulites. *Journal of Geology* **95,** 617–632.

Bohlen, S. R. & Liotta, J. L. (1986). A barometer for garnet amphibolites and garnet granulites. *Journal of Petrology* **27,** 1025–1034.

Bohlen, S. R., Wall, V. J. & Boettcher, A. (1983). Experimental investigations and geological applications of equilibria in the system $FeO–TiO_2–Al_2O_3–SiO_2–H_2O$. *American Mineralogist* **68,** 1049–1058.

Bohlen, S. R., Dollase, W. D. & Wall, V. J. (1986). Calibration and applications of spinel equilibria in the system $FeO–Al_2O_3–SiO_2$. *Journal of Petrology* **27,** 1143–1156.

Brown, M. (1993). *P–T–t* evolution of orogenic belts and the causes of regional metamorphism. *Journal of the Geological Society, London* **150,** 227–241.

Carl, C., Dill, H., Kreuzer, H. & Wendt, I. (1985). U/Pb und K/Ar-Datierungen des Uranvorkommens Hohenstein. *Geologische Rundschau* **74,** 483–504.

Carrington, D. P. & Harley, S. L. (1995). Partial melting and phase relations in high-grade metapelites: an experimental petrogenetic grid in the KFMASH system. *Contributions to Mineralogy and Petrology* **120,** 270–291.

Carrington, D. P. & Harley, S. L. (1996). Cordierite as a monitor of fluid and melt H_2O contents in the lower crust: an experimental calibration. *Geology* **24,** 647–650.

Carrington, D. P. & Watt, G. R. (1995). A geochemical and experimental study of the role of K-feldspar during water-undersaturated melting of metapelites. *Chemical Geology* **122,** 59–76.

Chakraborty, S. & Ganguly, J. (1990). Compositional zoning and cation diffusion in garnets. In: Ganguly, J. (ed.) *Diffusion, Atomic Ordering, and Mass Transport.* New York: Springer, pp. 120–175.

Chernoff, C. B. & Carlson, W. D. (1997). Disequilibrium for Ca during growth of pelitic garnet. *Journal of Metamorphic Geology* **15,** 421–438.

Clemens, J. D., Droop, G. T. R. & Stevens, G. (1997). High-grade metamorphism, dehydration and crustal melting: a reinvestigation based on new experiments in the silica-saturated portion of the system $KAlO_2–MgO–SiO_2–H_2O–CO_2$ at $P \leq 1{\cdot}5$ GPa. *Contributions to Mineralogy and Petrology* **129,** 308–325.

Connolly, J. A. D. & Cesare, B. (1993). C–O–H–S fluid composition and oxygen fugacity in graphitic metapelites. *Journal of Metamorphic Geology* **11,** 379–388.

Dasgupta, S., Sengupta, P., Ehl, J., Raith, M. & Bardhan, S. (1995). Reaction textures in a suite of spinel granulites from the Eastern Ghats Belt, India: evidence for polymetamorphism, a partial petrogenetic grid in the system KFMASH and the roles of ZnO and Fe_2O_3. *Journal of Petrology* **36,** 435–461.

England, P. C. & Thompson, A. B. (1986). Some thermal and tectonic models for crustal melting in continental collision belts. In: Coward, M. P. & Ries, A. C. (eds) *Collision Tectonics. Geological Society, London, Special Publications* **19,** 83–94.

Fischer, G. & Troll, G. (1973). Bauplan und Gefügeentwicklung metamorpher und magmatischer Gesteine des Bayerischen Waldes. *Geologica Bavarica* **68,** 7–44.

Fitzsimons, I. C. W. (1996). Metapelitic migmatites from Brattstrand Bluffs, East Antarctica—metamorphism, melting and exhumation of the mid crust. *Journal of Petrology* **37,** 395–414.

Franke, W. (1989). Tectonostratigraphic units in the Variscan belt of Europe. *Geological Society of America, Special Papers* **230,** 67–90.

Gardien, V., Thompson, A. B., Grujic, D. & Ulmer, P. (1995). Experimental melting of biotite + plagioclase + quartz ± muscovite assemblages and implications for crustal melting. *Journal of Geophysical Research* **100**(B8), 15581–15591.

Gerdes, A., Wörner, G. & Finger, F. (1995). Quellen und Prozesse der Genese des Südböhmischen Batholiths. *Terra Nostra* **95**(8), 97.

Grauert, B., Hänny, R. & Soptranajowa, G. (1974). Geochronology in a polymetamorphic and anatectic gneiss region: the Moldanubicum of the area Lam–Deggendorf, eastern Bavaria, Germany. *Contributions to Mineralogy and Petrology* **45,** 37–63.

Greenfield, J. E., Clarke, G. L. & White, R. W. (1998). A sequence of partial melting reactions at Mt Stafford, central Australia. *Journal of Metamorphic Geology* **16,** 363–378.

Harley, S. L. (1984). An experimental study of the partitioning of Fe and Mg between garnet and orthopyroxene. *Contributions to Mineralogy and Petrology* **86,** 359–373.

Harley, S. L. (1989). The origins of granulites: a metamorphic perspective. *Geological Magazine* **126,** 215–331.

Hensen, B. J. & Green, D. H. (1973). Experimental study of the stability of cordierite and garnet in pelitic compositions at high pressures and temperatures III. Synthesis of experimental data and geological applications. *Contributions to Mineralogy and Petrology* **38,** 151–166.

Johannes, W. & Schreyer, W. (1981). Experimental introduction of CO_2 and H_2O into Mg-cordierite. *American Journal of Science* **281,** 299–317.

Kalt, A., Grauert, B. & Baumann, A. (1994*a*). Rb–Sr and U–Pb studies on migmatites from the Schwarzwald (F.R.G.): constraints on isotopic resetting during high-temperature metamorphism. *Journal of Metamorphic Geology* **12,** 667–680.

Kalt, A., Hanel, M., Schleicher, H. & Kramm, U. (1994*b*). Petrology and geochronology of eclogites from the Variscan Schwarzwald (F.R.G.). *Contributions to Mineralogy and Petrology* **115,** 287–302.

Kalt, A., Altherr, R. & Ludwig, T. (1998). Contact metamorphism in pelitic rocks on the island of Kos (Greece, Eastern Aegean Sea): a test for the Na-in-cordierite thermometer. *Journal of Petrology* **39,** 663.

Keppler, H. (1989). The influence of the fluid phase composition on the solidus temperatures in the haplogranite system $NaAlSi_3O_8$–$KAlSi_3O_8$–SiO_2–H_2O–CO_2. *Contributions to Mineralogy and Petrology* **102,** 321–327.

Komatsu, M., Toyoshima, T., Osanai, Y. & Arai, M. (1994). Prograde and anatectic reactions in the deep arc crust exposed in the Hidaka metamorphic belt, Hokkaido, Japan. *Lithos* **33,** 31–49.

Kossmat, F. (1927). Gliederung des varistischen Gebirgebaus. *Abhandlungen der Sächsischen Geologischen Landesanstalt* **1,** 1–39.

Koziol, A. M. & Newton, R. C. (1988). Redetermination of the anorthite breakdown reaction and improvement of the plagioclase–garnet–Al_2SiO_5–quartz geothermobarometer. *American Mineralogist* **73,** 216–223.

Kretz, R. (1983). Symbols for rock-forming minerals. *American Mineralogist* **68,** 277–279.

Kreuzer, H., Seidel, E., Schüssler, U., Okrusch, M., Lenz, K. & Raschka, H. (1989). K–Ar geochronology of different tectonic units at the NW margin of the Bohemian Massif. *Tectonophysics* **157,** 149–178.

Langer, C., Hegner, E., Altherr, R., Satir, M. & Henjes-Kunst, F. (1995). Carboniferous granitoids from the Odenwald, the Schwarzwald and the Vosges Mts.: constraints on mantle and crustal sources. *Terra Nostra* **95**(8), 114.

Le Breton, N. & Thompson, A. B. (1988). Fluid-absent (dehydration) melting of biotite in metapelites in the early stages of crustal anatexis. *Contributions to Mineralogy and Petrology* **99,** 226–237.

Loomis, T. P. (1986). Metamorphism of metapelites: calculation of equilibrium assemblages and numerical simulations of the crystallization of garnet. *Journal of Metamorphic Geology* **4,** 201–230.

Martignole, J. & Sisi, J. C. (1981). Cordierite–garnet–H_2O equilibrium: a geological thermometer, barometer, and water fugacity indicator. *Contributions to Mineralogy and Petrology* **77,** 38–46.

Masch, L. & Cetin, B. (1991). Gefüge, Deformationsmechanismen und Kinematik in ausgewählten HT-Mylonitzonen im Moldanubikum des Bayerischen Waldes. *Geologica Bavarica* **96,** 7–26.

Matte, P. (1986). Tectonics and plate tectonics model for the Variscan belt in Europe. *Tectonophysics* **126,** 329–374.

Medaris, L. G., Jelínek, E. & Mísar, Z. (1995). Czech eclogites: terrane settings and implications for Variscan tectonic evolution of the Bohemian Massif. *European Journal of Mineralogy* **7,** 7–28.

Medaris, L. G., Fournalle, J. H., Ghent, E. D., Jelínek, E. & Mísar, Z. (1998). Prograde eclogite in the Gföhl Nappe, Czech Republic: new evidence on Variscan high-pressure metamorphism. *Journal of Metamorphic Geology* **16,** 563–576.

Mirwald, P. (1986). Ist Cordierit ein Geothermometer? *Fortschritte der Mineralogie* **64**(Beiheft 1), 119.

Montel, J.-M. & Vielzeuf, D. (1997). Partial melting of metagreywackes, Part II. Compositions of minerals and melts. *Contributions to Mineralogy and Petrology* **128,** 176–196.

Mukhopadhyay, B. & Holdaway, M. J. (1994). Cordierite–garnet–sillimanite–quartz equilibrium: I. New experimental calibration in the system FeO–Al_2O_3–SiO_2–H_2O and certain P–T–X_{H2O} relations. *Contributions to Mineralogy and Petrology* **116,** 462–472.

O'Brien, P. J. & Carswell, D. A. (1993). Tectonometamorphic evolution of the Bohemian Massif: evidence from high-pressure metamorphic rocks. *Geologische Rundschau* **82,** 531–555.

Patiño Douce, A. E. & Beard, J. S. (1995). Dehydration-melting of biotite gneiss and quartz amphibolite from 3 to 15 kbar. *Journal of Petrology* **36,** 707–738.

Patiño Douce, A. E. & Beard, J. S. (1996). Effects of P, $f(O_2)$ and Mg/Fe ratio on dehydration melting of model metagreywackes. *Journal of Petrology* **37,** 999–1024.

Patiño Douce, A. E. & Johnston, A. D. (1991). Phase equilibria and melt productivity in the pelitic system: implications for the origin of peraluminous granitoids and aluminous granulites. *Contributions to Mineralogy and Petrology* **107,** 202–218.

Pitra, P. (1996). Étude pétrostructurale des régions marginales du Moldanubien de Bohême et de ses relations avec le bloc du Barrandien. Ph.D. Thesis, Muséum National d'Histoire Naturelle, Paris.

Poulson, S. R. & Ohmoto, H. (1989). Devolatilization equilibria in graphite–pyrite–pyrrhotite bearing pelites with application to magma–pelite interaction. *Contributions to Mineralogy and Petrology* **101,** 418–425.

Raith, J. G. & Harley, S. L. (1998). Low-*P*/high-*T* metamorphism in the Okiep Copper District, western Namaqualand, South Africa. *Journal of Metamorphic Geology* **16,** 281–305.

Schaltegger, U. & Corfu, F. (1996). Dating short-lived late orogenic extensional events in the Variscan belt of central Europe. *Journal of Conference Abstracts* **1,** 538.

Schreyer, W. & Blümel, P. (1974). Progressive metamorphism in the Moldanubicum of the Northern Bavarian Forest. *Fortschritte der Mineralogie* **52**(Beiheft 1), 151–165.

Schreyer, W., Kullerud, G. & Ramdohr, P. (1964). Metamorphic conditions of ore and country rock of the Bodenmais, Bavaria, sulfide deposit. *Neues Jahrbuch für Mineralogie Abhandlungen* **101,** 1–26.

Shi, P. (1992). Fluid fugacities and phase equilibria in the Fe–Si–O–H–S system. *American Mineralogist* **77,** 1050–1066.

Siebel, W. (1995). Anticorrelated Rb–Sr and K–Ar age discordances, Leuchtenberg granite, NE Bavaria, Germany. *Contributions to Mineralogy and Petrology* **120,** 197–211.

Skjerlie, K. P. & Johnston, A. D. (1993). Fluid-absent melting behaviour of an F-rich tonalitic gneiss at mid-crustal pressures: implications for the generation of anorogenic granites. *Journal of Petrology* **34,** 785–815.

Stevens, G., Clemens, J. D. & Droop, G. T. R. (1997). Melt production during granulite-facies anatexis: experimental data from 'primitive' metasedimentary protoliths. *Contributions to Mineralogy and Petrology* **128,** 352–370.

Tanner, D. C. & Behrmann, J. H. (1995). The Variscan tectonics of the Moldanubian gneisses, Oberpfälzer Wald: a compressional history. *Neues Jahrbuch für Geologie und Paläontologie* **197,** 331–355.

Teufel, S. (1988). Vergleichende U–Pb- und Rb–Sr-Altersbestimmungen an Gesteinen des Übergangsbereiches Saxothuringikum/Moldanubikum, NE Bayern. *Göttinger Arbeiten zur Geologie und Paläontologie* **35,** 87 pp.

Thompson, A. B. & Connolly, A. D. (1995). Melting of the continental crust: some thermal and petrological constraints on anatexis in continental collision zones and other tectonic settings. *Journal of Geophysical Research* **100**(B8), 15565–15579.

Troll, G. (1967). Geologische Übersichtskarte des Bayerischen Waldes 1:100 000. *Supplement to Geologica Bavarica* **58**.

Troll, G. (1968). Geologische Übersichtskarte des Regensburger Waldes 1:100 000. *Supplement to Geologica Bavarica* **59**.

Turnock, A. C. & Eugster, H. P. (1962). Fe–Al oxides: phase relationships below 1,000°C. *Journal of Petrology* **3,** 533–565.

Vielzeuf, D. & Holloway, J. (1988). Experimental determination of the vapor-absent melting relations in the pelitic system. *Contributions to Mineralogy and Petrology* **98,** 257–276.

Vielzeuf, D. & Montel, J. M. (1994). Partial melting of metagreywackes, I, Fluid-absent experiments and phase relationships. *Contributions to Mineralogy and Petrology* **118,** 375–394.

Waters, D. J. (1991). Hercynite–quartz granulites: phase relations, and implications for crustal processes. *European Journal of Mineralogy* **3,** 367–386.

Wells, P. R. A. (1977). Pyroxene thermometry in simple and complex systems. *Contributions to Mineralogy and Petrology* **62,** 129–139.

Wendt, I., Kreuzer, H., Müller, P. & Schmid, H. (1986). Gesamtgesteins- und Mineraldatierungen des Falkenberger Granits. *Geologisches Jahrbuch* **E34,** 5–66.

Whittington, A., Harris, N. & Baker, J. (1998). Low-pressure crustal anatexis: the significance of spinel and cordierite from metapelitic assemblages at Nanga Parbat, northern Pakistan. In: Treloar, P. J. & O'Brien, P. J. (eds) *What Drives Metamorphism and Metamorphic Reactions? Geological Society, London, Special Publications* **138,** 183–198.

Zoubek, V. (1965). Das Moldanubikum und seine Stellung im geologischen Bau Europas. *Freiberger Forschungshefte* **C190,** 129–148.